microRNA-142 is critical for the homeostasis and function of type-1 innate lymphoid cells

Melissa M. Berrien-Elliott[1], **Yaping Sun**[2], **Carly Neal**[1], **Aaron Ireland**[1], **Maria C. Trissal**[1], **Ryan P. Sullivan**[1,†], **Julia A. Wagner**[1], **Jeffrey W. Leong**[1], **Pamela Wong**[1], **Annelise Y. Mah-Som**[3], **Terrence N. Wong**[1], **Timothy Schappe**[1], **Catherine R. Keppel**[1], **Victor S. Cortez**[4], **Efstathios G. Stamatiades**[5], **Ming O. Li**[5], **Marco Colonna**[4], **Daniel C. Link**[1], **Anthony R. French**[3], **Megan A. Cooper**[3], **Mark P. Boldin**[6], **Pavan Reddy**[2], **Todd A. Fehniger**[*,1,7]

[1]Department of Medicine, Division of Oncology, Washington University School of Medicine, Saint Louis, MO, USA

[2]Division of Hematology/Oncology, University of Michigan, Ann Arbor, MI, USA

[3]Department of Pediatrics, Division of Rheumatology, Washington University School of Medicine, Saint Louis, MO, USA

[4]Department of Pathology and Immunology, Washington University School of Medicine, Saint Louis, MO, USA

[5]Immunology Program, Memorial Sloan Kettering Cancer Center, New York, New York 10065, USA

[6]Department of Molecular and Cellular Biology, Beckman Research Institute of the City of Hope, Duarte, CA, USA

[7]Lead Contact.

Summary

Natural killer (NK) cells are cytotoxic type-1 innate lymphoid cells (ILCs) that defend against viruses and mediate anti-tumor responses, yet mechanisms controlling their development and function remain incompletely understood. We hypothesized that the abundantly expressed microRNA-142 is a critical regulator of type-1 ILC biology. Interleukin (IL)-15 signaling induced miR-142 expression, while global and ILC-specific miR-142-deficient mice exhibited a cell-intrinsic loss of NK cells. Death of NK cells resulted from diminished IL-15-receptor signaling within miR-142-deficient mice, likely via reduced suppressor of cytokine signaling-1 (Socs1)

[*]Correspondence to: tfehnige@wustl.edu.

Author contributions: M.M.B-E. and T.A.F. conceived and designed the study; Y.S. P.R., M.P.B., E.G.S., and M.L. provided critical reagents; M.M.B-E., A.I., M.T., R.P.S., C.C.N., P.W., J.A.W., J.W.L., A.Y.M-S., T.W., T.S., C.R.K., D.L., E.S., M.C., V.C, M.A.C., A.R.F., M.A.C., and T.A.F. collected, analyzed, and assembled data; M.M.B-E. and T.A.F. wrote the manuscript; and all authors reviewed the data, edited and approved the final version of the manuscript.
[†]Present address: Novartis Institutes for Biomedical Research, 250 Massachusetts Ave., Cambridge, Massachusetts 02139, USA.

regulation by miR-142-5p. ILCs persisting in *Mir142⁻/⁻* mice demonstrated increased expression of the miR-142-3p-target αV integrin, which supported their survival. Global miR-142-deficient mice exhibited an expansion of ILC1-like cells concurrent with increased transforming growth factor-β (TGF-β) signaling. Further, miR-142-deficient mice had reduced NK cell-dependent function and increased susceptibility to MCMV infection. Thus, miR-142 critically integrates environmental cues for proper type-1 ILC homeostasis and defense against viral infection.

Graphical Abstract
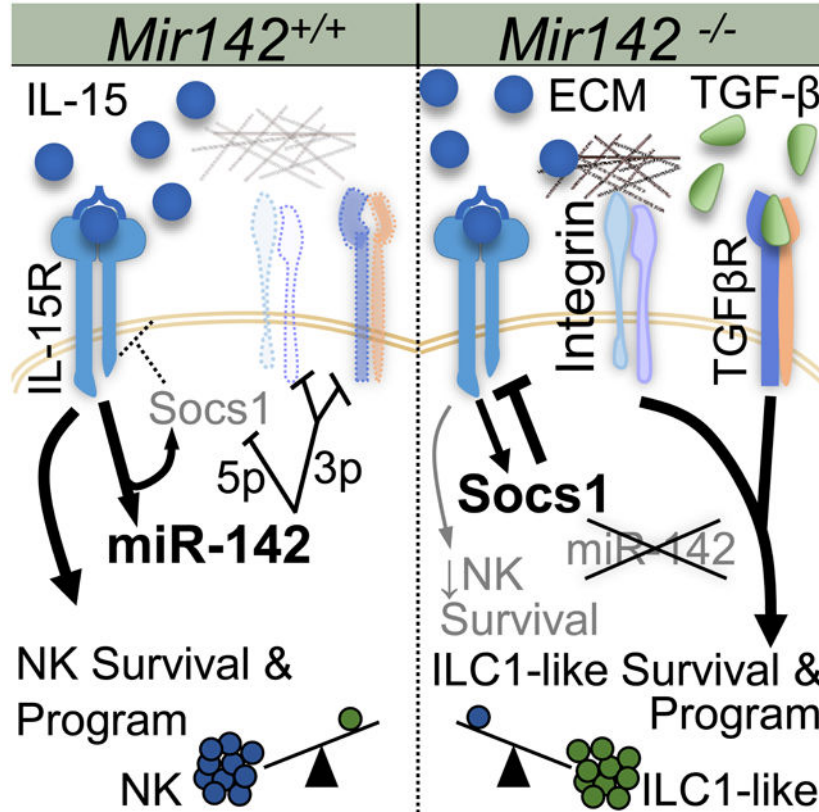
eTOC

IL-15 and TGF-β support the homeostasis and molecular programs of distinct innate lymphoid cell (ILC) types. Berrien-Elliott and colleagues identify that microRNA-142 is required for IL-15 receptor signaling and NK cell survival, while loss of microRNA-142 results in distinct TGF-β– and/or integrin-supported type-1 ILCs.

Keywords

NK cells; innate lymphoid cells; ILC1-like cells; microRNA-142; IL-15; integrin; tissue resident; cytokine receptors; murine cytomegalovirus

Introduction

Type-1 innate lymphoid cells (ILCs) include natural killer (NK) cells, ILC1s, and ILC-1-like cells, which have distinct and overlapping properties. NK cells are important for controlling viral infections and eliminating malignant cells (Vivier et al., 2008). To protect the host, NK cells both release cytokines (e.g. IFN-γ) and kill target cells (Lanier, 2008). Like NK cells, ILC1s produce interferon-γ (IFN-γ) in response to cytokine receptor signals but localize to different sites in vivo and are poorly cytotoxic. NK cells are found throughout lymphoid organs and tissues, whereas ILC1 cells are found primarily in non-lymphoid tissues (Diefenbach et al., 2014). ILC1-like cells have been described in the salivary gland with a discrete phenotype and transcriptional signature (Cortez et al., 2014, 2016, 2017). Although the functions of ILC1 and ILC1-like cells are incompletely understood, evidence suggests they are important for limiting T cell-mediated tissue damage and potentially eliminating virally-infected cells (Cortez et al., 2016; Schuster et al., 2014; Weizman et al., 2017). Other tissue-resident, non-cytotoxic ILCs (ILC 2 and 3) are classified based on the types of cytokines produced and transcription factors required for their development and survival (Diefenbach et al., 2014).

Although the common lymphoid progenitor (CLP) gives rise to T, B, NK and ILCs, NK cells and ILCs are distinct from adaptive T and B cells in both development and function (Yokoyama et al., 2004). NK cell development and education progress in the bone marrow (BM) and secondary lymphoid organs and result in the generation of functionally-competent effector cells (Orr and Lanier, 2010). Recent studies support that ILC1s develop from a precursor down-stream of the CLP and have a transcriptional profile distinct from NK cells (Daussy et al., 2014). During development, both restricted NK cell precursors and type-1 ILCs acquire the IL-2 and -15Rβ chain (CD122), enabling them to respond to the cytokine IL-15, which supports their development, homeostasis (Klose et al., 2014; Marçais et al., 2013), and function (Fehniger et al., 2007). In addition, ILC1 and ILC1-like phenotypes and effector functions may depend on factors within the tissue microenvironment where they reside, especially TGF-β. TGF-β has been shown to drive the generation of a unique subset of ILC1-like cells normally present in the salivary glands (Cortez et al., 2014, 2016, 2017) and can convert NK cells into ILC1-like cells within the tumor microenvironment (Gao et al., 2017). Despite advances in NK cell and ILC biology, the molecular mechanisms controlling their development and homeostasis remain incompletely understood. In particular, while transcriptional regulators of type-1 ILC development have been defined, many post-transcriptional facets of their molecular programs remain unclear (Leong et al., 2016).

MicroRNAs (miRNAs) are small non-coding RNAs that regulate protein production, classically via binding to specific sites in the 3' untranslated region (UTR) of target mRNAs, thereby preventing their translation or promoting their degradation (Lewis et al., 2005). A large number of individual miRNAs are expressed by NK cells; however, ~50 sequences comprise the majority of mature miRNA sequence content (Fehniger et al., 2010). Furthermore, several miRNAs or miRNA families regulate various aspects of NK cell and ILC biology (Leong et al., 2016; Singh et al., 2017). The conserved *mir142* gene encodes two highly-expressed mature miRNAs, 142-3p and 5p, that are processed from the same

precursor yet have different mRNA targets. A role for miR-142-3p/5p in regulating hematopoietic cells has been reported using global $Mir142^{-/-}$ mouse models, and is variable depending on the cells examined. Megakaryocytes, mast cells, dendritic cells, and erythrocytes require miR-142 for their development and function and previous reports have demonstrated a reduction in peripheral T cells and altered B cell development in miR-142-deficient mice (Chapnik et al., 2014; Kramer et al., 2015; Mildner et al., 2013; Rivkin et al., 2017; Yamada et al., 2014). miR-142-3p/5p have been also shown to be important for mature T cell effector responses and proliferation (Sun et al., 2015). However, the role of miR-142-3p/5p in type-1 ILC development and function has not been previously reported. Since miR-142-3p and −5p were highly expressed in NK cells, we hypothesized that these miRNAs coordinately regulate type-1 ILC biology. To test this, both global $Mir142^{-/-}$ and ILC-specific mouse models were examined, which revealed a profound impact of miR-142-deficiency on normal type-1 ILC development and homeostasis.

Results

mir-142 deficiency reduces peripheral type-1 ILC cell numbers

To define the importance of miR-142 in the development and persistence of CD45$^+$CD3$^-$ NK1.1$^+$NKp46$^+$ type-1 ILCs that include NK cells, ILC1s, and ILC1-like cells, $Mir142^{-/-}$ mice were examined. NK1.1$^+$NKp46$^+$ cell numbers were significantly reduced in the blood, spleen (SP), liver (LV), and lymph nodes (LN) of $Mir142^{-/-}$ mice, compared to control ($Mir142^{+/+}$) mice. In contrast, the total BM NK1.1$^+$ cell number was not altered (Fig. 1 A-B, Fig. S1). The reduction of type-1 ILCs in the periphery was unlikely to result from a block in maturation, because miR-142-3p and −5p mature miRNA sequences were expressed throughout NK cell maturation (Fig. S2), and the relative frequencies of maturation stage II-IV NK1.1$^+$ cells were unchanged in $Mir142^{-/-}$ mice (Fig. S1).

To establish a cell-intrinsic requirement of miR-142 for normal NK1.1$^+$ cell numbers, mixed BM chimera experiments were performed. Congenic BM cells (CD45.2$^+$ $Mir142^{-/-}$ and CD45.1 $Mir142^{+/+}$ WT) were transferred into irradiated WT CD45.1$^+$CD45.2$^+$ recipients at a 4:1 or 1:1 ratio and NK1.1$^+$ cell chimerism was assessed in the BM and spleen after 6-12 weeks (Fig. 1C-D). As a control, WT CD45.2$^+$ and WT CD45.1$^+$ BM were transferred into irradiated recipients at the same ratios. If NK1.1$^+$ cells require miR-142 in a cell-intrinsic manner, different NK1.1$^+$ cell frequencies were expected between mice that received WT:WT and $Mir142^{-/-}$:WT BM. Marked reductions in the frequency of NK1.1$^+$ cells derived from the $Mir142^{-/-}$ BM donor were observed at both ratios, compared to the $Mir142^{+/+}$ donors, in the BM and spleen of recipient mice (Fig. 1D). Congenic mice reconstituted with $Mir142^{-/-}$ BM in non-competitive transplantation demonstrate a similar reduction in NK1.1$^+$ cells developing from the transferred $Mir142^{-/-}$ BM compared to controls (Fig. 1E). While BM pre-NK cell precursors (pre-NKP, Lin$^-$CD27$^+$CD244$^+$CD122$^-$CD127$^+$FLT3$^-$) do not differ in total numbers between $Mir142^{-/-}$ and control mice, restricted NK precursors (rNKp, Lin$^-$CD27$^+$CD244$^+$CD122$^+$CD127$^+$FLT3−), which depend on IL-15, are significantly reduced (Fig. 1F) (Fathman et al., 2011). CLPs are confirmed as being unaltered in $Mir142^{-/-}$ BM compared to controls (Fig. S3) (Sun et al., 2015). Collectively, these data indicate that

miR-142 is required in a cell-intrinsic manner for the homeostasis of peripheral NK1.1$^+$ cells, and the maintenance of the rNKp in the BM.

mir-142 deficiency alters type-1 ILC trafficking in vivo

Altered trafficking from the BM could contribute to the pattern of type-1 ILCs deficiency observed in *Mir142$^{-/-}$* mice. In order to investigate this, whole BM cells containing equivalent numbers of NK1.1$^+$ cells from control and *Mir142$^{-/-}$* mice were differentially labeled, mixed at a 1:1 ratio, and injected into recipient mice (Fig. 1G). After 16 hours, the spleen, BM, liver, blood, lung, LN and salivary gland (SG) were assessed for the ratio of transferred control:*Mir142$^{-/-}$* NK1.1$^+$NKp46$^+$ cells (Fig. 1H-I). Trafficking defects in *Mir142$^{-/-}$* BM NK1.1$^+$ cells to the spleen, BM and LN of recipient mice were observed, while preferential trafficking of *Mir142$^{-/-}$* BM NK1.1$^+$ cells to the liver and lung of recipient mice was evident (Fig. 1H-I). Transferred NK1.1$^+$NKp46$^+$ cells (both WT and *Mir142$^{-/-}$*) were not detected in the SG. Blood NK1.1$^+$ cell frequency was similar between *Mir142$^{-/-}$* and control cells after mixed BM adoptive transfer. These data indicate that the *Mir142$^{-/-}$* type-1 ILCs preferentially trafficked to non-lymphoid tissues and led to the hypothesis that NK1.1$^+$ cells that persist in *Mir142$^{-/-}$* mice have tissue-resident properties.

Mir142$^{-/-}$ mice are deficient in NK cells but accumulate ILC1-like cells

Type-1 ILCs may be categorized based on expression of CD49a (integrin α1) and CD49b (integrin α2) as NK cells (CD49a-CD49b$^+$), tissue-resident ILC1s (CD49a$^+$CD49b−), and SG ILC1-like cells (CD49a$^+$CD49b$^+$) (Cortez et al., 2016; Gasteiger et al., 2015; Sojka et al., 2014). To better define the type-1 ILC subsets impacted within *Mir142$^{-/-}$* mice, CD3$^-$NK1.1$^+$NKp46$^+$ cells were examined for CD49a and CD49b expression in lymphoid and non-lymphoid tissues (Fig. 2A-C). The majority of type-1 ILCs in the lymphoid tissues of *Mir142$^{-/-}$* mice expressed both CD49a and CD49b, consistent with ILC1-like cells (Fig. 2A-B). This analysis also revealed marked reductions in NK cells in the BM, spleen, SG (all 10% of controls) and liver (20% of controls) of *Mir142$^{-/-}$* mice compared to controls (Fig. 2B). In contrast, *Mir142$^{-/-}$* mice have expansions of ILC1-like cells in BM (where they matched NK cell numbers within control mice), spleen, and liver (Fig. 2A-B). *Mir142$^{-/-}$* mice had reduced ILC1-like cells in the SG where they normally predominate in WT mice (Fig. 2A-B). ILC1 numbers were not substantially altered by miR-142-deficiency in the liver where they normally reside. However, ILC1s were significantly reduced in the SG in *Mir142$^{-/-}$* mice compared to controls (Fig. 2B). Finally, mature miR-142-3p and −5p sequences were expressed throughout the type-1 ILC compartment in both mice and humans (Fig. S2) (Collins et al., 2019). Thus, in *Mir142$^{-/-}$* mice a complex and tissue-specific impact on type-1 ILCs is evident.

To confirm whether *Mir142$^{-/-}$* type-1 ILCs within lymphoid tissues exhibited characteristics of ILC1-like cells, additional markers were examined. CD43 is normally reduced on SG ILC1-like cells (Cortez et al., 2014), and was also decreased on *Mir142$^{-/-}$* NK1.1$^+$NKp46$^+$ cells (Fig. 3A-B). CD73 and TIGIT were increased on NK1.1$^+$NKp46$^+$ cells from *Mir142$^{-/-}$* mice compared to controls, also consistent with an SG ILC1-like phenotype (Fig. 3C). Finally, we examined Nfil3, T-bet, and Eomes, transcription factors important for type-1 ILC differentiation. While Nfil3 and T-bet were similar between the type-1 ILC subsets in the

spleen of *Mir142*^{−/−} and control mice, ILC1-like cells from *Mir142*^{−/−} mice also expressed Eomes similarly to control NK cells (Fig. 3D). Thus, while many cell surface marker alterations are shared between *Mir142*^{−/−} ILCs and ILC1-like cells, Eomes expression is more similar to NK cells.

Mice with ILC-specific deletion of miR-142 are deficient in NK cells

To better define the impact of intrinsic miR-142 deficiency on type-1 ILCs, an ILC-specific miR-142 deficient mouse was generated by crossing mice with a *Mir142*-floxed (*Mir142*[f/f]) allele (Kramer et al., 2015) with Cre-recombinase under the *Ncr1* (Nkp46)-promoter (Narni-Mancinelli et al., 2011). A reporter Lox-Stop-Lox flanked YFP allele genetically targeted into the *Rosa26* locus was used to track Cre activity (Srinivas et al., 2001) (*Ncr1-cre*[+] *Mir142*[f/f]) These mice revealed that miR142-3p/5p were critical for the development for NK, ILC1, and ILC1-like cells (Fig. 2C). However, the accumulation of ILC1-like cells observed in the global *Mir142*^{−/−} was abrogated, with only a modest accumulation of ILC1-like cells observed in the BM. This suggested that ILC-extrinsic factors also amplified the ILC1-like accumulation in global *Mir142*^{−/−} mice (Fig. 2C). To determine the extrinsic versus intrinsic contributions of miR-142-deficiency, we performed mixed BM chimera experiments (Fig. 2D-E), where WT (CD45.1[+]) and (*Ncr1-cre*[+] *Mir142*[f/f]) BM were mixed at a 1:1 ratio and transferred into irradiated WT or *Mir142*^{−/−} recipients. After 6 weeks, the splenic type-1 ILC compartment was assessed. WT cells developing in *Mir142*^{−/−} mice displayed a greater frequency of ILC1-like cells compared to WT cells in control mice (Fig. 2E). Overall these data support the hypothesis that *Mir142* is critical for orchestrating NK, ILC1-like, and ILC1 homeostasis. We further investigated ILC1-like cells from the global *Mir142*^{−/−} mice to better understand the extrinsic mechanisms that contribute to their persistence.

TGF-β signaling and molecular program are increased in Mir142^{−/−} type-1 ILC

TGF-β receptor signaling is involved in the development of ILC1-like cells in the SG (Cortez et al., 2016, 2017), and also resulted in CD49a expression on NK1.1^{+} cells within a tumor microenvironment (Gao et al., 2017). We hypothesized that TGF-β contributed to the ILC-1-like phenotype and performed gene expression analysis of sorted type-1 ILCs from *Mir142*^{−/−} and WT control mice. Gene set enrichment analysis (GSEA) revealed that *Mir142*^{−/−} NK1.1^{+} cells from the spleen and BM had significantly enriched genes associated with TGF-β receptor signaling (Fig. 4A). Next, the gene signatures of *Mir142*^{+/+}, *Mir142*^{−/−} and *Smad4*[/] NK1.1^{+} cells (Cortez et al., 2017) were compared. The ILC-1-like gene signature from *Smad4*[/] mice was evident within *Mir142*^{−/−} NK1.1^{+} cells, including *Il21r*, *Tnfsf10*, *Inpp4b*, *Itga1* up-regulation, and Sell and Mcam down-regulation, compared to controls (Fig. 4B). Murine *Tgfbr1* 3'UTR was confirmed as a direct biochemical target of miR-142-3p using luciferase reporter assays (Fig. 4C-D) (Lei et al., 2014). TGFBR1 was also increased on splenic NK1.1[+] NKp46^{+} cells in *Mir142*^{−/−} mice compared to controls (Fig. 4E). Finally, pSMAD-2 and/or −3 were increased in unstimulated and IL-15 and TGF-β-stimulated *Mir142*^{−/−} NK1.1^{+} cells compared to controls (Fig. 4F-G). Consistent with the presence of residual splenic NK cells and minimal ILC1s or ILC1-like cells (Fig. 2C), an increase in TGFBR1 or pSMAD-2 and/or −3 signaling was not evident in splenic NK cells from mice with ILC-specific miR-142 deletion, compared to controls (Fig. S4). However, significantly increased ILC1-like cells in the Ncr1-cre[+] *Mir142*[f/f] BM (Fig. 2C) and the

increased ILC1-like cells developing from Ncr1-cre[+] *Mir142[f/f]* BM in the WT environment (Fig. 2E), suggest a cell-intrinsic contribution of miR-142-3p to the ILC1-like phenotype. Collectively, these data suggest that miR-142 directly targeted *Tgfbr1* in vivo, which resulted in enhanced TGF-β receptor signaling, and a type-1 ILC molecular program overlapping with ILC1-like cells. When contrasted to the ILC-specific miR-142-deficient phenotype, these data indicate that a cell-extrinsic mechanism contributes to the ILC1-like phenotype of type-1 ILCs observed in global *Mir142^{−/−}* mice.

miR-142-deficient type-1 ILCs are hyporesponsive to IL-15 signaling

Since IL-15 is a central regulator of type-1 ILC homeostasis, the impact of IL-15 signaling on miR-142-3p/5p expression within NK1.1^{+} cells was examined. Splenic NK1.1^{+} cells from WT mice stimulated with IL-15 demonstrated a significant increase in miR-142-3p and −5p over time (Fig. 5A). These data suggested that elimination of miR-142 may impact IL-15 receptor (IL-15R) signaling feedback mechanisms, which could then alter IL-15-induced survival or proliferation. Baseline proliferation and expression of the anti-apoptotic molecule Bcl-2 were similar between controls and persisting *Mir142^{−/−}* NK1.1^{+} cells (Fig. S5), suggesting that these were not mechanisms that contributed to the phenotype. To assess survival, control or *Mir142^{−/−}* splenocytes were incubated for 48 hours with 1 or 10 ng/mL of IL-15 and NK1.1[+]NKp46^{+} cell viability was measured (Fig. 5B). Increased NK1.1[+] cell death of *Mir142^{−/−}* spleens compared to controls indicated that *Mir142^{−/−}* NK1.1^{+} cells had a reduced survival capacity when supported by IL-15 ex vivo. Thus, *Mir142^{−/−}* NK1.1^{+} cells may have altered IL-15 signaling, a critical cytokine for type-1 ILC survival and homeostasis (Cortez et al., 2014; Klose et al., 2014; Ma et al., 2006; Marçais et al., 2013). The expression of the key IL-15R signaling components within *Mir142[f/f]* and control NK1.1^{+} cells were examined and no differences in the abundance of IL-2 and −15Rβ or γ_c mRNA were detected (data not shown). However, IL-2 and −15Rβ (CD122) protein expression had a modest but significant reduction in MFI on *Mir142^{−/−}* and *Ncr1-cre[+]Mir142[f/f]* BM and splenic NK1.1^{+} cells, compared to controls. There was also a modest decrease in γ_c (CD132) MFI on *Mir142^{−/−}* NK1.1^{+} cells in the spleen (Fig. 5C-D, Fig. S5C-D). As a control, NK1.1 MFI was unaltered between *Mir142^{−/−}* and control NK1.1^{+} cells from the BM or spleen (Fig. S5). A primary IL-15R signal for NK cell survival is transduced via the JAK and STAT pathway, leading to STAT5 phosphorylation (Marçais et al., 2013). mRNA expression of proximal IL-15R JAK and STAT signaling molecules was unaltered in *Mir142^{−/−}* mice (Fig. S6). *Mir142^{−/−}* or *Ncr1-cre[+] Mir142[f/f]* splenocytes were stimulated with IL-15 and STAT5 (Y694) phosphorylation assessed (Fig. 5E-F). There was a sustained, significant reduction in pSTAT5 MFI in NK1.1^{+} cells following IL-15 stimulation from the *Mir142^{−/−}* mice, compared to controls (Fig. 5F). The *Ncr1-cre[+] Mir142[f/f]* type-1 ILCs also had significantly diminished STAT5 phosphorylation in response to IL-15. Further, since *Mir142^{−/−}* ILCs signaled excessively through the TGF-βR, we hypothesized that TGF-β negatively impacts NK cell survival. Consistent with this, WT NK1.1[+] cell death increased when TGF-β was present in the culture system (Fig. S5). Together, these data support the idea that *Mir142^{−/−}* NK1.1^{+} cells fail to sufficiently signal through the IL-15R, leading to reduced survival in vivo. *Mir142^{−/−}*, *Ncr1-cre[+] Mir142[f/f]* and control splenocytes were also stimulated with IL-12 for 15 minutes and STAT4 phosphorylation was assessed (Fig. 5G-H). We detected reduced pSTAT4 (Y693) in response to IL-12 in both global and ILC-specific

miR-142-deficient NK cells (Fig. 5G-H). These data suggested that a general mechanism led to broad reduction in JAK and STAT signaling in the absence of miR-142.

Socs1 is a direct target of miR-142-5p in type-1 ILCs

Although IL-15Rβ protein expression was mildly reduced on miR-142-deficient NK1.1^{+} cells compared to controls, this modest change in surface density was unlikely to explain the lack of STAT5 phosphorylation in response to IL-15. Consistent with findings in human macrophages (Su et al., 2015), the murine *Socs1* 3'UTR was a direct target of miR-142-5p (Fig. 5I). Increased *Socs1* expression would be expected to result in abrogated IL-15-induced JAK and STAT signaling and consequently cell death. Flow-sorted NK1.1^{+} cells from the spleen of *Mir142*^{−/−} mice expressed increased Socs1 protein immediately ex vivo (Fig. 5J-K). The modest extent of Socs1 protein increase was expected, since type-1 ILC with increased Socs1 protein would diminish IL-15 survival signals and die, as evidenced by in vivo loss of this compartment (Figs. 1-2). Collectively, these data support the hypothesis that miR-142-5p maintains physiologic IL-15 responsiveness (and hence survival) in peripheral NK1.1^{+} cells via targeting *Socs1*.

Integrin αV promotes type-1 ILC cell survival in miR-142-deficient mice

Since all type-1 ILCs depend on IL-15 for survival in WT mice (Diefenbach et al., 2014), our findings raised an important question: how do type-1 ILCs persist in *Mir142*^{−/−} mice when IL-15-induced pSTAT5 was compromised? *Il15*^{−/−} mice have residual NK1.1^{+} cells that persist in the BM and were thought to be immature (Yoshizawa et al., 2011). Consistent with previous reports, *Il15*^{−/−} mice had a markedly reduced type-1 ILCs (Fig. S3). However, a reproducible CD3^{−} NK1.1^{+}NKp46^{+}CD49b^{+} cell population was detected within the spleen of *Il15*^{−/−} mice. These residual type-1 ILCs expressed significantly increased integrin αVβ3 and CD49a (Fig. 6A, Fig. S3). Increased integrin αV was also detected in the BM, spleen, and liver of type-1 ILCs from *Mir142*^{−/−} and *Ncr1-cre*[+] *Mir142*[f/f] mice compared to controls (Fig. 6B-C). Moreover, bioinformatic analyses revealed that the 3' UTR of *Itgav*, the gene that encodes integrin αV (CD51) protein, was a predicted target of miR-142-3p. The *Itgav* 3' UTR was directly targeted by miR-142-3p (Fig. 6D). We hypothesized that signaling through the vitronectin and fibronectin receptor (αVβ3) may promote NK cell survival when IL-15 signaling is diminished. To test this, *Mir142*^{−/−} mice were treated with an integrin αV antagonist (cilengetide) for two weeks, and then the type-1 ILC compartment of the spleen was assessed (Reardon et al., 2008). A significant decrease in type-1 ILCs was observed in the treated *Mir142*^{−/−} mice compared to control-treated *Mir142*^{−/−} mice (Fig. 6E). Collectively, these data suggest that integrin αV expression is regulated by miR-142-3p and promotes type-1 ILC survival in the absence of normal IL-15R signaling, providing a mechanism for the survival of persisting type-1 ILCs in miR-142-deficient mice.

miR-142-deficient type-1 ILC display altered effector responses in vitro and in vivo

We next assessed the functional impact of miR-142-deficiency on NK1.1^{+} cells in vitro and in vivo. Although ILC1s and ILC1-like cells are not considered highly cytotoxic, they can degranulate and produce IFN-γ in response to cytokine stimulation or activating receptor ligation (Cortez et al., 2016; Sojka et al., 2014). Splenocytes from *Mir142*^{−/−}, *Ncr1-cre*[+] *Mir142*[f/f] and control mice were stimulated with IL-12 plus IL-15 and NK1.1^{+} cells were

assessed for IFN-γ production (Figure 7A-D). Compared to controls, $Mir142^{-/-}$ type-1 ILCs exhibited a marked reduction in IFN-γ production in response to cytokine co-stimulation (Fig. 7A-B). While ILC1- like cells have been shown to produce less IFN-γ than NK cells, the reduction was modest (~10%) (Cortez et al., 2017). ILC1-like cells from the SG in control mice produced markedly reduced amounts of IFN-γ in response to cytokine stimulation, similar to $Mir142^{-/-}$ NK1.1^{+} splenocytes (Fig. S7). In addition, NK1.1^{+} cells within $Mir142^{-/-}$ mice exhibited reduced IFN-γ responses and degranulation to activating receptor ligation and failed to effectively kill TRAIL-sensitive target cells in a standard flow-based killing assay (Fig. S7). These data suggest that type-1 ILCs that persist in the setting of miR-142-deficiency fail to mediate the normal pattern of type-1 ILC functions.

$Mir142^{-/-}$ NK1.1^{+} cells have impaired responses to MCMV infection in vivo

Since $Mir142^{-/-}$ ILC1-like cells are hypofunctional in vitro, we hypothesized that $Mir142^{-/-}$ mice have a compromised response to viral infection in vivo. Consistent with this, type-1 ILCs from $Mir142^{-/-}$ mice exhibited reduced IFN-γ production following polyI:C injection (Fig. S7) and murine cytomegalovirus (MCMV) infection (Fig. 7E-F). Following MCMV infection, $Mir142^{-/-}$ mice had significantly increased viral loads in the spleen compared to control mice (Fig. 7G). This resulted in host susceptibility and death following a normally sub-lethal dose of MCMV (Fig. 7H). Overall, these data indicated that miR-142 is critical for normal type-1 ILC effector functions in vivo.

Discussion

Here we report that a single miRNA gene is essential for the cell-intrinsic development and homeostatic composition of the type-1 ILC compartment. miR-142 was expressed within developing and mature type-1 ILCs from WT mice and its transcription was induced by IL-15R signaling. Loss of miR-142 resulted in a marked reduction of type-1 ILCs that was evident in both global and ILC-specific genetic deletion models. One mechanism contributing to the type-1 ILC reduction was compromised IL-15R signaling and survival. This was likely due to release of the negative regulator of IL-15 signaling, Socs1, from normal miR-142-5p regulation. In global $Mir142^{-/-}$ mice, while NK cells were nearly absent, an expansion of ILC1-like cells in lymphoid tissues was evident. By contrasting global and ILC-specific miR-142 deletion, a cell-extrinsic mechanism was identified that contributed to this aberrant ILC1-like accumulation in lymphoid tissues. $Tgfbr1$ was found to be targeted by miR-142-3p, and TGF-β signaling was increased in $Mir142^{-/-}$ type-1 ILCs, which promoted the ILC1-like phenotype observed in these mice. While IL-15 signaling was markedly diminished, some type-1 ILCs survived in miR-142-deficient mice. Integrin αV was expressed on persisting type-1 ILCs, and αV antagonists resulted in loss of these cells in vivo, identifying a previously unreported role for integrins to compensate for reduced IL-15R survival signals in type-1 ILCs. These data support the idea that type-1 ILC survival and composition is influenced by both an intrinsic molecular program and the tissue environment, including the cytokine milieu and extracellular matrix (ECM) composition. Collectively, the type-1 ILC alterations in miR-142-deficient mice, which included a profound loss of normal NK cell effector functions, resulted in loss of host protection and

survival following viral infection. Thus, miR-142 is vital for normal type-1 ILC homeostasis and function.

This study revealed both cell-intrinsic and cell-extrinsic effects of miR-142 deficiency on type-1 ILCs. Several mechanisms contribute to the change from NK cells to ILC1-like cells in $Mir142^{-/-}$ mice, with ILC-specific miR-142 deficiency clarifying that the loss of NK cells is intrinsic, while the accumulation of ILC-1-like cells was promoted by extrinsic factors. One mechanism was the increased responsiveness to TGF-β by type-1 ILCs. Increased TGF-β signaling has been shown to be detrimental to NK cells, inducing cell death and reducing mTOR signaling (Viel et al., 2016). Consistent with this, miR-142-deficiency nearly eliminated the NK cells normally present in lymphoid tissues. Also in line with enhanced TGF-β signaling in $Mir142^{-/-}$ mice, normally tissue-resident ILC1-like cells expanded in the lymphoid tissues and displayed a TGF-β molecular signature. Loss of miR-142-3p targeting of $Tgfbr1$ in $Mir142^{-/-}$ mice was associated with increased TGFBR1 expression and TGF-β signaling in expanded ILC1-like cells. Since the ILC1-like accumulation was restricted to the BM of ILC-specific miR-142-deleted mice, and transfer of WT BM into $Mir142^{-/-}$ resulted in increased ILC1-like cells, $Mir142^{-/-}$ mice have an ILC-extrinsic increase in TGF-β availability in vivo. Studies report that TGF-β is critical for promoting the ILC1-like phenotype in the SG and within the tumor microenvironment, where NK cells were converted to ILC1-like cells (Cortez et al., 2017; Gao et al., 2017). It will be of interest to investigate the role of miR-142 in these models of ILC1-like cell promotion in future studies.

Our results indicate that miR-142-5p normally supports NK cells by promoting IL-15-based homeostatic survival signals by directly targeting $Socs1$. Indeed, the persisting $Mir142^{-/-}$ NK1.1^{+} cells expressed increased Socs1 protein in vivo and miR-142-deficient type-1 ILCs displayed severely reduced STAT5 phosphorylation concomitant with alterations in this pathway. Observing normal ILC1 numbers in the liver and an accumulation of ILC1-like cells in the $Mir142^{-/-}$ mouse model was not predicted since all type-1 ILCs depend on IL-15 for survival in WT mice (Diefenbach et al., 2014). $Ncr1$-cre[+] $Mir142^{f/f}$ mice, which also had deficient IL-15R signaling, did display reductions in the type-1 ILC compartment consistent with the requirement of these cells for IL-15. These differences suggest that there are IL-15-independent mechanisms that can support type-1 ILC survival, and integrin receptor signaling was identified as one mechanism. Mir142-deficient type-1 ILCs express integrin α1 and αV, similar to WT tissue-resident type-1 ILCs (but not NK cells). Integrins interacting with fibronectin (αVβ1) and vitronectin (αVβ3) have been reported to promote expression of the anti-apoptotic molecule BCL-2 (Matter and Ruoslahti, 2001; Zhang et al., 1995), similar to the IL-15R (Cooper et al., 2002). These integrin ligands are abundant in the ECM within the BM (Nilsson et al., 1998), where integrin αV[+] type-1 ILCs may receive survival signals that compensate for the reduced IL-15R signaling in miR-142-deficient mice. Previous reports identified that type-1 ILCs in $Il15^{-/-}$ mice display an "immature" αV[+] phenotype in the BM. An alternative explanation, supported by our analyses of $Il15^{-/-}$ mice, is that αV integrin selectively supports the survival of type-1 ILCs when IL-15 signals were limited. Here, type-1 ILCs were reduced in number when integrin αV was inhibited in $Mir142^{-/-}$ mice in vivo, where IL-15 signaling is also diminished. Linking this concept to the TGF-β signal enhancement in $Mir142^{--}$ mice, TGF-β is important for SG organogenesis

and regulates ECM deposition, including collagens and fibronectin (Hall et al., 2010; Ignotz and Massague, 1986), as well as promoting the collagen receptor VLA-1 (CD49a or $\alpha 1\beta 1$) on type-1 ILCs (Cortez et al., 2016). VLA-1 expressed by ILC1s and ILC1-like cells bind to collagen, which could play a role in promoting survival. Under homeostatic conditions in the LN, lymphocytes do not access collagen, which is ensheathed by fibroblastic reticular cells (Roozendaal et al., 2008). Consistent with a requirement for collagen binding, ILC1-like cells in $Mir142^{-/-}$ mice could not accumulate or survive in the LN microenvironment. This is also consistent with integrin expression and type–1 ILC phenotype of persisting NK1.1^{+} cells within $Mir142^{-/-}$ mice being promoted by factors within the tissue microenvironment (e.g. TGF-β) and encounters with vitronectin, fibronectin, and collagen in ECM. Such integrin signaling would be especially important for persistence in IL-15-low and TGF-β-rich microenvironments. Collectively, these findings indicate that integrin signaling provides an alternative pro-survival signal for type-1 ILCs, compensating for reduced cytokine survival signals, and warrants further investigation.

Previous studies have demonstrated that miRNAs are involved in NK cell maturation and effector functions (Bezman et al., 2011; Leong et al., 2016; Sullivan et al., 2015). miR-155 is modestly expressed in resting NK cells, but induced upon activation, and has previously been shown to regulate IFN-γ production and NK cell survival in mice, but only in the setting of activation or an immune response to infection. Mice lacking miR-155 have normal peripheral type-1 ILC numbers (Sullivan et al., 2013; Zawislak et al., 2013), but $Mir155^{-/-}$ NK cells failed to expand in response to MCMV infection, intriguingly due to $Socs1$ regulation (Lu et al., 2015; Zawislak et al., 2013). In contrast, $Mir142^{-/-}$ mice appear to have a marked alteration in the NK1.1^{+} cell compartment and function at baseline during normal homeostasis, consistent with the abundant expression of these miRNAs throughout NK cell development. Thus, from an evolutionary standpoint, Socs1 represents a key homeostatic feedback mechanism in type-1 ILCs, kept in check during normal homeostasis by miR-142, and by miR-155 only after robust activation. Studies in ILC2 revealed that the miR-17~92 family regulates $Socs1$ as well (Singh et al., 2017), suggesting a conserved requirement for miRNA regulation of this molecule within the ILC compartment. CIS, another suppressor of cytokine signaling family member, has been identified as an important negative regulator of IL-15 signaling in NK cells (Delconte et al., 2016). In a global deletion model, $Cish^{-/-}$ NK cells display enhanced survival. In that study, Socs1 was shown to be more efficient at preventing JAK1 signal transduction, compared to CIS, demonstrating how potent Socs1 may be at regulating IL-15R signaling (Delconte et al., 2016). Thus, multiple miRNA regulation mechanisms of cytokine receptor feedback appear to be an important aspect of maintaining type-1 ILCs during both homeostasis and response to infection.

In summary, studying type-1 ILCs within miR-142-deficient mice revealed a critical, non-redundant role for miR-142-3p/5p in regulating homeostatic NK cell, ILC1, and ILC1-like cell numbers, as well as responses to IL-15, other cytokines, and viral infection. Thus, miR-142 expression is required for the homeostasis and normal effector responses of type-1 ILCs.

STAR METHODS

CONTACT FOR REAGENTS AND RESOURCE SHARING

Further information and requests for resources and reagents should be directed to and will be fulfilled by the lead contact, Todd A. Fehniger (tfehnige@wustl.edu).

EXPERIMENTAL MODEL AND SUBJECTS DETAILS

Mice—The C57BL/6J *Mir142*$^{-/-}$ (Sun et al., 2015), *Mir142*$^{f/f}$(Kramer et al., 2015), *Ncr1-icre* (Narni-Mancinelli et al., 2011), and IL-15-deficient (Kennedy et al., 2000) mice have been previously described and are crossed to the C57BL/6 background. C57BL/6J mice were wild-type controls (Jackson Laboratory), and CD45.1 and CD45.2 F1 mice were obtained from C57BL/6J × CD45.1 (Taconic Farms) crosses. All mice were bred and maintained in specific, pathogen-free housing, and all experiments were conducted in accordance with the guidelines of and approval by the Washington University Animal Studies Committee. Male and female mice aged 8-12 weeks were used in each experiment, mice were age- and sex-matched per experiment, and then randomly allocated into experimental groups. Data from all mice are reported, thus there are no exclusion criteria to report.

Cell lines—The 293T cells (gift from M. Sands, Washington University School of Medicine) were maintained in complete DMEM supplemented (10% FBS, 10mM HEPES, 1% NEAA, 1% sodium pyruvate, 1% L-glutamine, 1X penicillin and streptomycin) and 3T3 (ex vivo killing assays) were obtained from ATCC. Cells were grown at 37° in 5% CO_2 in supplemented media, per ATCC instructions.

Virus—Viruses and injection of mice salivary gland stock of Smith strain MCMV (ATCC) was prepared using young BALB/c mice that were injected i.p. with 1×106 PFU tissue-culture propagated MCMV, viral titer was determined using standard plaque assay in NIH3T12 fibroblasts (ATCC). Unless otherwise indicated, mice were injected with 1×10^5 PFU.

METHOD DETAILS

Cell isolation—Mouse tissues were isolated from mice and processed as previously described (Cortez et al., 2016; Leong et al., 2015). For this study, the axillary, brachial, and inguinal LN were harvested, pooled and processed. Briefly, blood was obtained from cardiac puncture and placed into EDTA tubes. Blood was lysed using 1X ACK lysis buffer (2 minutes at room temperature) and washed in PBS. Spleens and lymph nodes were crushed through a 70μM filter and RBC lysed using 1X ACK lysis buffer and washed in PBS. Livers were homogenized and washed with PBS, lymphocytes were obtained using percoll gradient. Salivary glands were digested with collagenase for 45 minutes at 37 °, then crushed through a 70μM filter. Lymphocytes were obtained by percoll gradient. Bone marrow was obtained from the femur by flushing PBS through the bone with a 23G needle. RBCs were lysed with 1X ACK lysis buffer and washed with PBS. All lymphocytes were resuspended in RPMI supplemented with 10% FBS, filtered through mesh, and stored on ice as needed.

Antibodies—The following anti-mouse antibodies were used for flow cytometry analysis as previously described: CD3 (500A2), NK1.1 (PK136), CD45 (30-F11), CD11c (HL3), CD49a (Ha31/8), CD29 (Ha2/5), CD51 (RMV-7), CD49f (GoH3), B7 (M293), CD11a (2D7), Ly-49 C/I (5E6), Ly49 A (A1), Ly-49 D (4E5), Ly-6G/C (Gr1, RB6-8C5), Ly-76 (TER-119), CD132 (4G3), CD135 (FLT-3, A2F10.1), IFN-γ (XMG1.2), pSTAT4 pY693, pSTAT5 pY694, FcBlock (2.4G2), Annexin V, 7-AAD, CD49d (R1-2), CD18 (C71/16), CD61 (2C9.G2), pSMAD2/3 (O72-670), TIGIT (1G9) from BD Biosciences; CD107a (1D4B) from Beckman Coulter; anti-Rabbit IgG from Cell Signaling Technology; CD27 (LG.7F9) CD11b (M1/70), CD122 (TM-β1), CD49b (DX5), Ly49 G2 (eBio4D11), LY-49 H (3D10), NKG2A (B6, 16a11), NKG2D (CX5), Ki67 (SolA15), B220 (RA3-6B2), CD127 (A7R34), Ly6D (49-H4), CD73 (eBioTY/11.8) from Affymetrix/eBioscience.

Quantification of MCMV viral loads using real-time PCR—MCMV viral loads were determined by quantifying the copies of the IE1 gene using qRT-PCR (TaqMan) as previously described (Fogel et al., 2013). Tissue pieces (5 mm^3) were minced and placed in Gentra Puregene Cell Lysis Buffer (Qiagen), and DNA was extracted following the manufacturer's recommended protocol and diluted to 20–50ng/ml. MCMV immediate-early gene 1 (ie1)-specific primers and probe were used to determine viral copy number as described and normalized to β-actin (*Actb*). Reactions were run in duplicate on a 7500 Fast Real-Time PCR instrument (Applied Biosystems) with an absolute standard curve. The limit of reliable detection using the standard was 100 copies of MCMV, and all values below 100 were rounded up. Graphs represent ([copies MCMV *ie1*]/[copies *Actb*]) × 1,000. Statistics were performed on log-transformed data.

IFN-γ assays—IFN-γ stimulations were performed as previously described (Sullivan et al., 2012). Briefly, 1×10^6 splenocytes were stimulated with recombinant IL-12 and IL-15 (10 ng/mL each; PreproTech) or anti-NK1.1 (plate-bound PK136, 5μg/mL) in complete RPMI for 6 hours in the presence of anti- CD107a. After 1 hour, golgiPlug and golgiStop (BD Biosciences) were added to each well and the cells incubated for an additional 5 hours. Mice were inoculated with 1×10^5 plaque forming units (p.f.u.) of MCMV (Smith strain, salivary gland stock) ip. and spleens harvested 36 hours later and splenocytes assessed for intracellular IFN-γ. Splenic processing and surface staining were performed on ice, immediately after harvest. For intracellular staining, BD CytoFix/CytoPerm kit was used according to manufacturer's instructions.

In vivo trafficking assay—Whole BM cells were isolated from mice, labeled with cell trace (CT) violet or CT Yellow per manufacturers' protocol, mixed at a 1:1 ratio, and injected i.v. into the tail vein of recipient control mice. After 16 hours organs were harvested, enumerated, and assessed by flow cytometry for the relative abundance of labeled NK cells. In this assay, total BM cells were transferred due to limiting numbers of NK1.1$^+$ cells in the BM and equal NK1.1$^+$ cell number in control and *Mir142*$^{-/-}$ mice.

Ex vivo survival assay—To assess ex vivo viability, 1×10^6 splenocytes were incubated with 1 or 10 ng/mL IL-15 in complete RPMI for 48 hours. In indicated assays 10 ng/mL rhTGF-β1 (Peprotech) was added, as well. Cells were surface stained and viability assessed

by 7-Aminoactinomycin D incorporation (7-AAD; Sigma Aldrich) and Annexin V staining (BD biosciences, according to manufacturer's instructions).

Cytokine Signaling Assays—To assess cytokine signaling, 1×10^6 splenocytes were stimulated with IL-12 (10 ng/mL) for 15 minutes, or IL-15 (10 or 100 ng/mL) for 15, 30, and 60 minutes, or 10 ng/mL IL-15 plus 10 ng/mL TGF-β for 15, 30, and 60 minutes and immediately fixed in equal volume of pre-warmed 4% formaldehyde. After fixation for 10 minutes, cells were permeabilized with ice cold 100% methanol and incubated on ice for 30 minutes. Cells were surface stained 15 minutes prior to fixation (CD3 and NK1.1). Intracellular staining was performed overnight at 4°C with the indicated mAbs to detect phosphorylated STAT4, STAT5, or Smad-2 and/or −3.

miRNA 3'UTR reporter luciferase assays—Overexpression of miR-142 and luciferase sensor plasmids were performed as previously described (Fehniger et al., 2010; Sullivan et al., 2012). The wild-type *Socs1*, *Tgfbr1*, and the first 1Kb of the *Itgav* 3'UTR were cloned into the psiCheck2 vector (Promega). The miR142-3p and −5p sites were mutated as indicated using the QuikChange II Site-Directed mutagenesis Kit (Agilent Technologies) following manufacturer's instructions. miR-142-3p/5p pre-miRNA $^{+}$/− 200bp flanking genomic sequence was sub-cloned into the pMND overexpression vector (a gift from M. Sands) (Fehniger et al., 2010). All primer sequences used for cloning are available upon request. 293T cells were co-transfected with 400ng of each vector using Dharmafect Duo (Dharmacon). After 48 hours, the Dual-Glow Luciferase Assay (Promega) was performed according to manufacturer's instructions on an LD400 luminescence detector (Beckman Coulter). miR142 overexpression was confirmed by flow cytometry for GFP expression.

In vivo integrin αV inhibitor assays—Cilengitide (Sigma) was administered for 2 weeks (500 μg Cilengitide ip. on days 1-4, 7-11, 13) (Du et al., 2016). Vehicle control mice received PBS (HyClone).

Flow cytometry and sorting—All flow cytometry data were collected on a Gallios flow cytometer (Beckman Coulter). Data were analyzed using FlowJo (Tree Star) software. Cell sorting was performed on BD FACS Aria II to >95% purity.

mRNA expression analysis by microarray—Mononuclear cells were harvested from *Mir142*$^{+/+}$ or *Mir142*$^{-/-}$ spleen or BM and NK cells were sorted to >95% purity (NK1.1$^+$CD3$^-$). RNA was isolated using TRIzol (Invitrogen) according to manufacturer's instructions. 50ng of total RNA was used to generate biotinylated cDNA, according to the standard NuGen WT-Ovation Pico RNA Amplification kit. Following fragmentation with NuGen Encore Biotin Module, 2.5 ug of cDNA were hybridized onto Mouse Gene 1.0 ST Arrays in the GeneChip Hybridization Oven 640 for 18 hr at 45°C. GeneChips were then washed and stained in the Affymetrix Fluidics Station 450, and were scanned using the Affymetrix GeneChip 7G 3000 Scanner. The scanned raw .CEL files were analyzed to export signal intensity values, using Affymetrix Expression Console software with Affymetrix Gene Expression workflow using default settings. Differently expressed genes were determined using an ANOVA and significance was determined using a P value with an FDR < 0.05 (Partek Genomics Suite 6.6). Assays were performed in triplicate.

Gene Set Enrichment Analysis (GSEA)—Microarray .CEL files from control and $Mir142^{-/-}$ spleen and bone marrow were used for this analysis. Raw data .CEL files were imported into GenePattern analysis software (Broad Institute publicly available GenePattern server) where background correction and normalization were performed with standard default settings. The .CEL files were combined into one .gct file in GenePattern, then imported into GSEA along with a matching phenotype label file (.cls). GSEA analysis was run with the following parameters: number of permutations = 1000, collapse dataset to gene symbols = true, permutation type = gene_set, chip platform = MoGene_1_0_st.chip, plot graphs for the top sets of each phenotype = 150 (default= 20), gene sets database = h.all.v6.0 symbols.gmt (all hallmarks, version 6), with a phenotype comparison of $Mir142^{-/-}$ versus control for SP and BM. Leading edge analysis was completed on the Hallmark GSEA output with TGF-beta signaling hallmark gene set.

Heat map generation—Gene sets were analyzed in Partek using the gene expression work flow. CEL. files from control and $Mir142^{-/-}$ spleen and bone marrow and the control and $Smad4^{-/-}$ gene set (GSE100247) were used for this analysis (Cortez et al., 2017). The ANOVA was completed with one comparison – wild-type and $Mir142^{-/-}$. The gene list was generated with > or = $^+/-$ 2-fold changes, P-value with FDR = 0.05. There were 159 Genes on the final list. The list of miR-142 predicted targets was generated with TargetScan Mouse, Release 7.1. There were 307 identified targets for 142-3p and 866 for 142–5p, and 42 unique genes were identified as targets for both 3p and 5p. A master list of targets was created, duplicate genes were removed, and the resulting 1128 miR-142 targets were compared to the list of 159 differentially expressed genes that was generated by Partek analysis. Eleven miR-142 targets were found on the Partek analysis list, and 8 of those are annotated on the heat map.

Western blot—Splenic and BM NK cells were sorted and >250,000, cells snap frozen using LN_2. Frozen pellets were then lysed on ice for 15 minutes using 1X RIPA buffer plus 1X Protease and phosphatase inhibitor cocktail (Cell Signaling). Lysates plus loading buffer (Cell Signaling) were boiled for 5 minutes and loaded into a Mini-PROTEAN TGX Precast 4-20% Gel (Bio-Rad). The gel was electrophoresed in 1X running buffer according to manufacturer's instructions. All gels were run with Precision plus protein western standard ladder (Bio-Rad). The proteins were transferred to 0.45 μM nitrocellulose using Mini Protean transfer apparatus (Bio-Rad) according to manufacturer's instructions. After transfer, the membrane was washed in TBS containing 0.1% Tween-20 (TBS-T) and blocked with TBS containing 5% FBS (Sigma) with agitation at room temperature for 1 hour. Blots were incubated with primary Socs1 (A156, Cell Signaling) or β-Actin (8H10D10, Cell signaling) antibodies overnight at 4°C with agitation. Blots were washed and incubated with anti-Rabbit or anti-Mouse HRP (Cell Signaling) for 60 minutes at room temperature. The blots were developed using the Super Signal West Femto Maximum sensitivity substrate according to manufacturer's instructions (ThermoScientific). All gels were imaged using BioRad Image Lab. Density was measured using BioRad Image Lab v 5.2.1 (BioRad). Relative well-loading was determined for $Mir142^{-/-}$ cells: control β-actin band intensity/ $Mir142^{-/-}$ band intensity = relative loading. Relative loading was then applied to the

measured $Mir142^{-/-}$ band intensity: relative loading x measured band intensity = normalized band intensity.

QUANTIFICATION AND STATISTICAL ANALYSIS

Normal distribution of data was determined by D'Agostino and Pearson omnibus normality test. If data were not normally distributed, the appropriate non-parametric test was performed. All figures depict mean, and uncertainty is represented in figures as standard error of the mean (SEM), unless otherwise indicated. All comparisons utilized a two-sided α of 0.05 for significance testing. Mouse blinding was not performed. Power analyses were not utilized, however, independent experiments were performed at least 2 times with a minimum of 3 mice in each group, and is indicated in the figure legends. All statistics were calculated in GraphPad Prism v8.0 software and are indicated in figure legends. P-values are expressed as follows: * p <0.05, ** p <0.01, *** p <0.001, **** p <0.0001.

DATA AND SOFTWARE AVAILABILITY

The microarray data are accessible within Gene Expression Omnibus (GEO) under accession code GSE85476.

Supplementary Material

Refer to Web version on PubMed Central for supplementary material.

Acknowledgments

References

Bezman NA, Chakraborty T, Bender T, and Lanier LL (2011). miR-150 regulates the development of NK and iNKT cells. J Exp Med 2018, 2717–2731.

Chapnik E, Rivkin N, Mildner A, Beck G, Pasvolsky R, Metzl-Raz E, Birger Y, Amir G, Tirosh I, Porat Z, et al. (2014). MiR-142 orchestrates a network of actin cytoskeleton regulators during megakaryopoiesis. Elife 3:e01964, 1–22. [PubMed: 24859754]

Collins PL, Cella M, Porter SI, Li S, Gurewitz GL, Hong HS, Johnson RP, Oltz EM, and Colonna M (2019). Gene Regulatory Programs Conferring Phenotypic Identities to Human NK Cells. Cell 176, 348–360.e12. [PubMed: 30595449]

Cooper MA, Bush JE, Fehniger TA, Vandeusen JB, Waite RE, Liu Y, Aguila HL, and Caligiuri MA (2002). In vivo evidence for a dependence on interleukin 15 for survival of natural killer cells. Blood 100, 3633–3638. [PubMed: 12393617]

Cortez VS, Fuchs A, Cella M, Gilfillan S, and Colonna M (2014). Cutting Edge: Salivary Gland NK Cells Develop Independently of Nfil3 in Steady-State. J. Immunol. 192, 4487–4491. [PubMed: 24740507]

Cortez VS, Cervantes-Barragan L, Robinette ML, Bando JK, Wang Y, Geiger TL, Gilfillan S, Fuchs A, Vivier E, Sun JC, et al. (2016). Transforming Growth Factor-β Signaling Guides the Differentiation of Innate Lymphoid Cells in Salivary Glands. Immunity 44, 1127–1139. [PubMed: 27156386]

Cortez VS, Ulland TK, Cervantes-Barragan L, Bando JK, Robinette ML, Wang Q, White AJ, Gilfillan S, Cella M, and Colonna M (2017). SMAD4 impedes the conversion of NK cells into ILC1-like cells by curtailing non-canonical TGF-β signaling. Nat. Immunol. 18, 995–1003. [PubMed: 28759002]

Daussy C, Faure F, Mayol K, Viel S, Gasteiger G, Charrier E, Bienvenu J, Henry T, Debien E, Hasan U a, et al. (2014). T-bet and Eomes instruct the development of two distinct natural killer cell lineages in the liver and in the bone marrow. J. Exp. Med. 211, 563–577. [PubMed: 24516120]

Delconte RB, Kolesnik TB, Dagley LF, Rautela J, Shi W, Putz EM, Stannard K, Zhang J-G, Teh C, Firth M, et al. (2016). CIS is a potent checkpoint in NK cell-mediated tumor immunity. Nat. Immunol. 17, 816–824. [PubMed: 27213690]

Diefenbach A, Colonna M, and Koyasu S (2014). Development , Differentiation , and Diversity of Innate Lymphoid Cells. Immunity 41, 354–365. [PubMed: 25238093]

Du F, Garg AV, Kosar K, Majumder S, Kugler DG, Mir GH, Maggio M, Henkel M, Lacy-Hulbert A, and McGeachy MJ (2016). Inflammatory Th17 Cells Express Integrin αvβ3 for Pathogenic Function. Cell Rep. 16, 1339–1351. [PubMed: 27452457]

Fathman JW, Bhattacharya D, Inlay MA, Seita J, Karsunky H, and Weissman IL (2011). Identification of the earliest natural killer cell-committed progenitor in murine bone marrow. Blood 118, 5439–5447. [PubMed: 21931117]

Fehniger TA, Cai SF, Cao X, Bredemeyer AJ, Presti RM, French AR, and Ley TJ (2007). Acquisition of murine NK cell cytotoxicity requires the translation of a pre-existing pool of granzyme B and perforin mRNAs. Immunity 26, 798–811. [PubMed: 17540585]

Fehniger TA, Wylie T, Germino E, Leong JW, Magrini VJ, Koul S, Keppel CR, Schneider SE, Koboldt DC, Sullivan RP, et al. (2010). Next-generation sequencing identifies the natural killer cell microRNA transcriptome. Genome Res 20, 1590–1604. [PubMed: 20935160]

Fogel LA, Sun MM, Geurs TL, Carayannopoulos LN, and French AR (2013). Markers of Nonselective and Specific NK Cell Activation. J Immunol 190, 6269–6276. [PubMed: 23656738]

Gao Y, Souza-Fonseca-Guimaraes F, Bald T, Ng SS, Young A, Ngiow SF, Rautela J, Straube J, Waddell N, Blake SJ, et al. (2017). Tumor immunoevasion by the conversion of effector NK cells into type 1 innate lymphoid cells. Nat. Immunol. 18, 1004–1015. [PubMed: 28759001]

Gasteiger G, Fan X, Dikiy S, Lee SY, Alexander Y, Program I, and Sloan M (2015). Tissue residency of innate lymphoid cells in lymphoid and non- lymphoid organs. Science (80-.). 350, 981–985.

Hall BE, Zheng C, Swaim WD, Cho A, Nagineni CN, Eckhaus MA, Flanders KC, Ambudkar IS, Baum BJ, and Kulkarni AB (2010). Conditional overexpression of TGF-B1 disrupts mouse salivary gland development and function. Lab. Investig. 90, 543–555. [PubMed: 20142803]

Ignotz R. a, and Massagué J (1986). Transforming growth factor-beta stimulates the expression of fibronectin and collagen and their incorporation into the extracellular matrix. J. Biol. Chem. 261, 4337–4345. [PubMed: 3456347]

Kennedy MK, Glaccum M, Brown SN, Butz E. a, Viney JL, Embers M, Matsuki N, Charrier K, Sedger L, Willis CR, et al. (2000). Reversible defects in natural killer and memory CD8 T cell lineages in interleukin 15-deficient mice. J. Exp. Med. 191, 771–780. [PubMed: 10704459]

Klose CSN, Flach M, Möhle L, Rogell L, Hoyler T, Ebert K, Fabiunke C, Pfeifer D, Sexl V, Fonseca-Pereira D, et al. (2014). Differentiation of type 1 ILCs from a common progenitor to all helper-like innate lymphoid cell lineages. Cell 157, 340–356. [PubMed: 24725403]

Kramer NJ, Wang W. Le, Reyes EY, Kumar B, Chen CC, Ramakrishna C, Cantin EM, Vonderfecht SL, Taganov KD, Chau N, et al. (2015). Altered lymphopoiesis and immunodeficiency in miR-142 null mice. Blood 125, 3720–3730. [PubMed: 25931583]

Lanier LL (2008). Evolutionary struggles between NK cells and viruses. Nat Rev Immunol 8, 259–268. [PubMed: 18340344]

Lei Z, Xu G, Wang L, Yang H, Liu X, Zhao J, and Zhang HT (2014). MiR-142-3p represses TGF-β-induced growth inhibition through repression of TGFβR1 in non-small cell lung cancer. FASEB J. 28, 2696–2704. [PubMed: 24558198]

Leong JW, Schneider SE, Sullivan RP, Parikh B. a, Anthony B. a, Singh A, Jewell B. a, Schappe T, Wagner J. a, Link DC, et al. (2015). PTEN regulates natural killer cell trafficking in vivo. Proc. Natl. Acad. Sci. 112, E700–E709. [PubMed: 25646418]

Leong JW, Wagner JA, Ireland AR, and Fehniger TA (2016). Transcriptional and post-transcriptional regulation of NK cell development and function. Clin. Immunol. 177, 60–69. [PubMed: 26948928]

Lewis BP, Burge CB, and Bartel DP (2005). Conserved seed pairing, often flanked by adenosines, indicates that thousands of human genes are microRNA targets. Cell 120, 15–20. [PubMed: 15652477]

Lu L-F, Gasteiger G, Yu I-S, Chaudhry A, Hsin J-P, Lu Y, Bos PD, Lin L-L, Zawislak CL, Cho S, et al. (2015). A Single miRNA-mRNA Interaction Affects the Immune Response in a Context- and Cell-Type-Specific Manner. Immunity 43, 52–64. [PubMed: 26163372]

Ma A, Koka R, and Burkett P (2006). Diverse functions of IL-2, IL-15, and IL-7 in lymphoid homeostasis. Annu. Rev. Immunol. 24, 657–679. [PubMed: 16551262]

Marçais A, Viel S, Grau M, Henry T, Marvel J, and Walzer T (2013). Regulation of Mouse NK Cell Development and Function by Cytokines. Front. Immunol. 4, 450. [PubMed: 24376448]

Matter ML, and Ruoslahti E (2001). A signaling pathway from the alpha5beta1 and alpha(v)beta3 integrins that elevates bcl-2 transcription. J Biol Chem 276, 27757–27763. [PubMed: 11333270]

Mildner A, Chapnik E, Manor O, Yona S, Kim KW, Aychek T, Varol D, Beck G, Itzhaki ZB, Feldmesser E, et al. (2013). Mononuclear phagocyte miRNome analysis identifies miR-142 as critical regulator of murine dendritic cell homeostasis. Blood 121, 1016–1027. [PubMed: 23212522]

Narni-Mancinelli E, Chaix J, Fenis A, Kerdiles YM, Yessaad N, Reynders A, Gregoire C, Luche H, Ugolini S, Tomasello E, et al. (2011). Fate mapping analysis of lymphoid cells expressing the NKp46 cell surface receptor. Proc. Natl. Acad. Sci. U. S. A. 108, 18324–18329. [PubMed: 22021440]

Nilsson SK, Debatis ME, Dooner MS, Madri JA, Quesenberry PJ, and Becker PS (1998). Immunofluorescence characterization of key extracellular matrix proteins in murine bone marrow in situ. J. Histochem. Cytochem. 46, 371–377. [PubMed: 9487119]

Orr MT, and Lanier LL (2010). Natural killer cell education and tolerance. Cell 142, 847–856. [PubMed: 20850008]

Reardon DA, Fink KL, Mikkelsen T, Cloughesy TF, O'Neill A, Plotkin S, Glantz M, Ravin P, Raizer JJ, Rich KM, et al. (2008). Randomized phase II study of cilengitide, an integrin-targeting arginine-glycine-aspartic acid peptide, in recurrent glioblastoma multiforme. J. Clin. Oncol.

Rivkin N, Chapnik E, Birger Y, Yanowski E, Curato C, Mildner A, Porat Z, Amir G, Izraeli S, Jung S, et al. (2017). Rac1 functions downstream of miR-142 in regulation of erythropoiesis. Haematologica 102, e476–e480. [PubMed: 28912177]

Roozendaal R, Mebius RE, and Kraal G (2008). The conduit system of the lymph node. Int. Immunol. 20, 1483–1487. [PubMed: 18824503]

Schuster IS, Wikstrom ME, Brizard G, Coudert JD, Estcourt MJ, Manzur M, O'Reilly LA, Smyth MJ, Trapani JA, Hill GR, et al. (2014). TRAIL$^+$ NK Cells Control CD4$^+$ T Cell Responses during Chronic Viral Infection to Limit Autoimmunity. Immunity 41, 646–656. [PubMed: 25367576]

Singh PB, Pua HH, Happ HC, Schneider C, von Moltke J, Locksley RM, Baumjohann D, and Ansel KM (2017). MicroRNA regulation of type 2 innate lymphoid cell homeostasis and function in allergic inflammation. J. Exp. Med.jem.20170545.

Sojka DK, Plougastel-Douglas B, Yang L, Pak-Wittel MA, Artyomov MN, Ivanova Y, Zhong C, Chase JM, Rothman PB, Yu J, et al. (2014). Tissue-resident natural killer (NK) cells are cell lineages distinct from thymic and conventional splenic NK cells. Elife 3, 1–21.

Srinivas S, Watanabe T, Lin CS, William CM, Tanabe Y, Jessell TM, and Costantini F (2001). Cre reporter strains produced by targeted insertion of EYFP and ECFP into the ROSA26 locus. BMC Dev Biol 1, 4. [PubMed: 11299042]

Su S, Zhao Q, He C, Huang D, Liu J, Chen F, Chen J, Liao J-Y, Cui X, Zeng Y, et al. (2015). miR-142-5p and miR-130a-3p are regulated by IL-4 and IL-13 and control profibrogenic macrophage program. Nat. Commun. 6, 8523. [PubMed: 26436920]

Sullivan R, Leong J, Schneider S, Ireland A, Berrien-Elliott M, Singh A, Schappe T, Jewell B, Sexl V, and Fehniger TA (2015). Mir-15/16 antagonizes Myb to control natural killer cell maturation. J Immunol 195, 2806–2817. [PubMed: 26268657]

Sullivan RP, Leong JW, Schneider SE, Keppel CKR, Germino E, French AR, and Fehniger TA (2012). MicroRNA Deficient NK Cells Exhibit Decreased Survival but Enhanced Function. J Immunol 188, 3019–3030. [PubMed: 22379033]

Sullivan RP, Fogel LA, Leong JW, Schneider SE, Wong R, Romee R, Thai T-H, Sexl V, Matkovich SJ, Dorn GW, et al. (2013). miR-155 tunes both the threshold and extent of NK cell activation via targeting of multiple signaling pathways. J Immunol 191, 5904–5913. [PubMed: 24227772]

Sun Y, Oravecz-Wilson K, Mathewson N, Wang Y, McEachin R, Liu C, Toubai T, Wu J, Rossi C, Braun T, et al. (2015). Mature T cell responses are controlled by microRNA-142. J. Clin. Invest. 125, 2825–2840. [PubMed: 26098216]

Viel S, Marçais A, Guimaraes FS, Loftus R, Rabilloud J, Grau M, Degouve S, Djebali S, Sanlaville A, Charrier E, et al. (2016). TGF- b inhibits the activation and functions of NK cells by repressing the mTOR pathway. 9, 1–14.

Vivier E, Tomasello E, Baratin M, Walzer T, and Ugolini S (2008). Functions of natural killer cells. Nat Immunol 9, 503–510. [PubMed: 18425107]

Weizman O. El, Adams NM, Schuster IS, Krishna C, Pritykin Y, Lau C, Degli-Esposti MA, Leslie CS, Sun JC, and O'Sullivan TE (2017). ILC1 Confer Early Host Protection at Initial Sites of Viral Infection. Cell.

Yamada Y, Kosaka K, Miyazawa T, Kurata-Miura K, and Yoshida T (2014). MiR-142-3p enhances Fc??RI-mediated degranulation in mast cells. Biochem. Biophys. Res. Commun. 443, 980–986. [PubMed: 24361879]

Yokoyama WM, Kim S, and French AR (2004). The dynamic life of natural killer cells. Ann Rev Immunol 22, 405–429. [PubMed: 15032583]

Yoshizawa K, Nakajima S, Notake T, Miyagawa S-I, Hida S, and Taki S (2011). IL-15-high-responder developing NK cells bearing Ly49 receptors in IL-15–/– mice. J. Immunol. 187, 43 5162–5169.

Zawislak CL, Beaulieu AM, Loeb GB, Karo J, Canner D, Bezman N. a, Lanier LL, Rudensky AY, and Sun JC (2013). Stage-specific regulation of natural killer cell homeostasis and response against viral infection by microRNA-155. Proc Natl Acad Sci USA 110, 6967–6972. [PubMed: 23572582]

Zhang Z, Vuori K, Reed JC, and Ruoslahti E (1995). The alpha 5 beta 1 integrin supports survival of cells on fibronectin and up-regulates Bcl-2 expression. Proc. Natl. Acad. Sci. U. S. A. 92, 6161–6165. [PubMed: 7541142]

Highlights

- miR-142 is induced by IL-15 and required for type-1 ILC development and homeostasis

- miR-142 targets SOCS1 thereby promotes IL-15 receptor signaling in type-1 ILCs

- αV integrin, a miR142-3p target, promotes IL-15-independent survival in type-1 ILCs

- miR-142 is critical for cytokine production and NK cell-mediated viral control
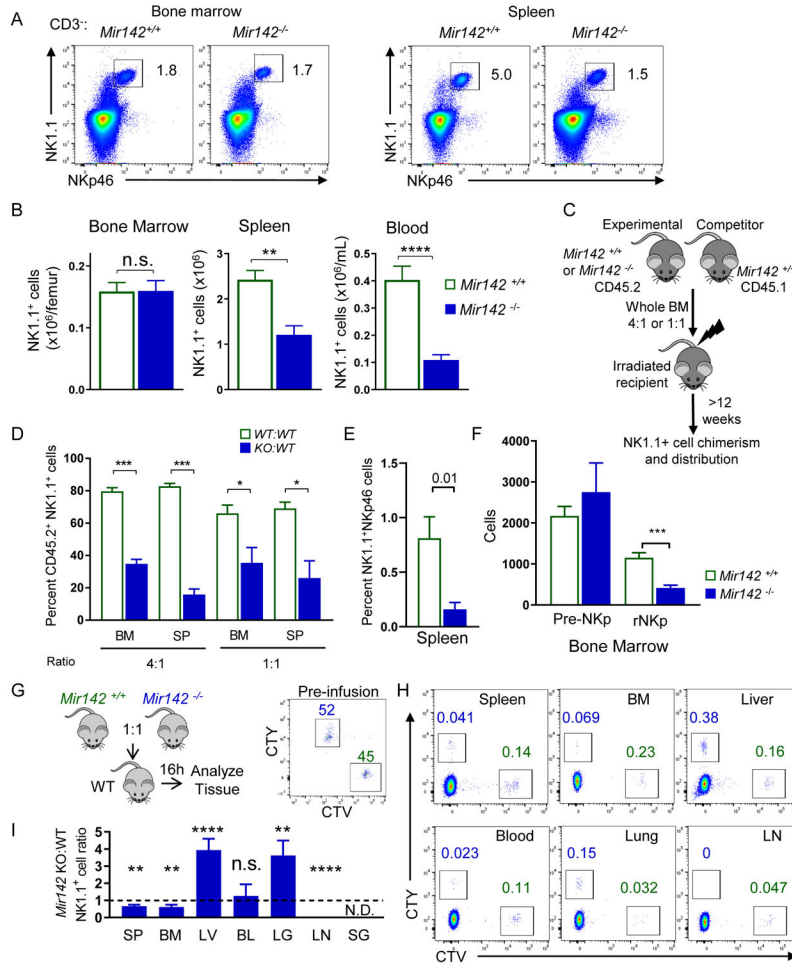
Figure 1. miR-142 deficiency reduces peripheral type-1 ILC numbers and alters trafficking.
BM, SP, and blood (BL) of *Mir142$^{+/+}$* (control, open green) and *Mir142$^{-/-}$* (filled blue) were
harvested and assessed for type-1 ILCs (CD45$^+$CD3$^-$NK1.1$^+$NKp46$^+$). (**A**) Representative
flow plot of NK1.1$^+$ NKp46$^+$ cells (gated on CD3$^-$) from the SP and BM. (**B**) Summary data
showing the total NK1.1$^+$ NKp46$^+$ cells, see Fig. S1 (**C-D**) Schema of the BM chimera
assay. (**D**) Summary of 2 independent experiments with >8 mice per group. (**E**) Non-
competitive BM chimera experiment where control or *Mir142$^{-/-}$* BM were transferred into
congenic, irradiated recipients. Summary data showing percent
CD45.2$^+$CD3$^-$NK1.1$^+$NKp46$^+$ cells from 3 independent experiments with 6 mice per group.
(**F**) Summary data showing the NK cell precursor population numbers: pre-NK precursor
(pre-NKp) and restricted NK precursor (rNKp). Data are from >3 independent experiments
with >12 mice per group. Data were compared using Student's T test or Mann-Whitney test.
(**G**) Experimental schema for trafficking experiments. Briefly, control and *miR142$^{-/-}$* BM
cells were differently labeled with cell trace violet and cell trace yellow. The cells were
mixed, injected iv. into WT recipients, and tissues examined for the presence of labeled
NK1.1$^+$NKp46$^+$ cells. Flow plots of pre-infusion NK1.1$^+$ cells present at 1:1 ratio. (**H**)
Representative flow cytometry showing NK1.1$^+$ cells. (**I**) Summary data from (H) showing
the ratio of control and *miR142$^{-/-}$* NK1.1$^+$ cells. N=10 mice from 2 independent

experiments. Significance was determined by Wilcoxon signed rank test against the theoretical value of one (no trafficking alteration, dashed line). Please also see Figure S3.
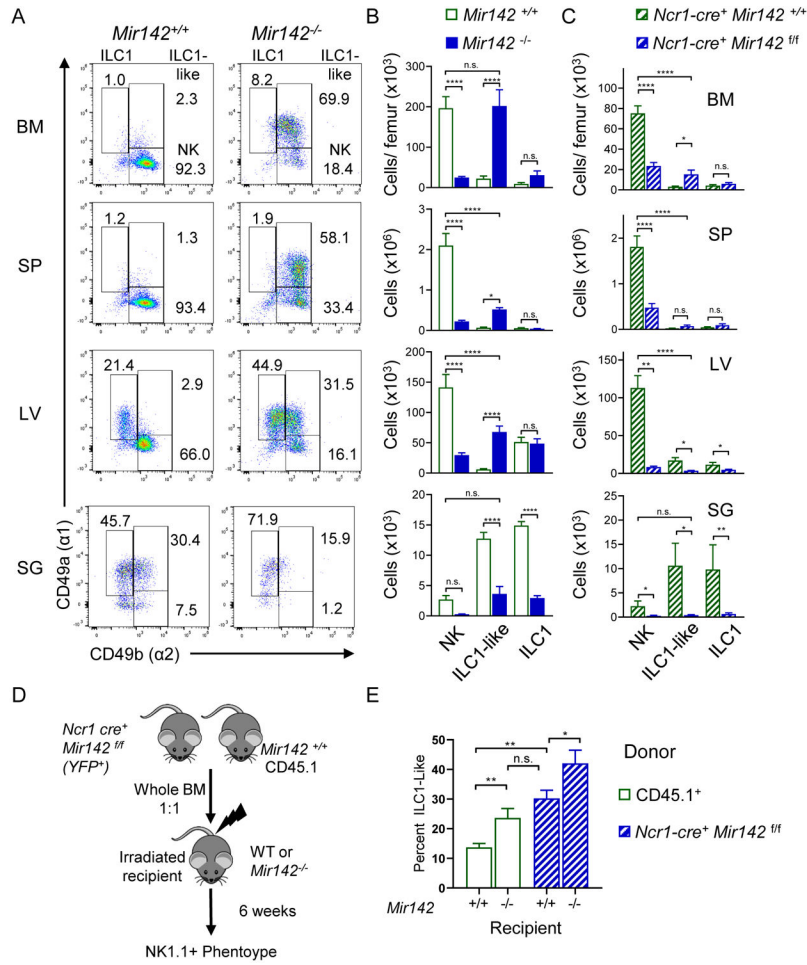
Figure 2. miR-142-deficient mice display altered, tissue-specific type-1 ILC compartment.
The CD3⁻NK1.1⁺NKp46⁺ compartment of *Mir142*^{+/+} (open green) and *Mir142*^{−/−} (filled blue) mice was assessed for CD49a and CD49b by flow cytometry. (**A**) Representative flow plots of CD3⁻NK 1.1 ⁺NKp46⁺ cells. (**B**) Total number of NK cells (NK, CD49a⁻CD49b⁺), ILC1-like (CD49a⁺CD49b⁺), and ILC1s (CD49a⁺CD49b⁻) within the indicated tissues. Summary from >3 independent experiments with > 10 mice per group. (**C**) Total numbers of NK, ILC1-like, and ILC1 cells within control (*Ncr1-cre*⁺ *Mir142*^{+/+}) and ILC-specific miR-142-deficient (*Ncr1-cre*⁺ *Mir142*^{f/f}) mice, cells gated on CD3⁻NK1.1⁺NKp46⁺ YFP⁺. (**D**) Experimental Schema. BM from control and *Ncr1-cre*⁺ *Mir142*^{f/f} mice were transferred into irradiated recipients and spleens assessed 6 weeks later. (**E**) Summary data showing the percent of ILC1-like cells from CD3-NK1.1⁺NKp46⁺ CD45.1⁺ (WT) or YFP⁺ (*Mir142*^{f/f}) within the indicated recipient mice. Data from 2-3 independent experiments, N=7-10 mice, compared using T-test or Mann-Whitney corrected for multiple comparisons, when appropriate. See also Figure S2.
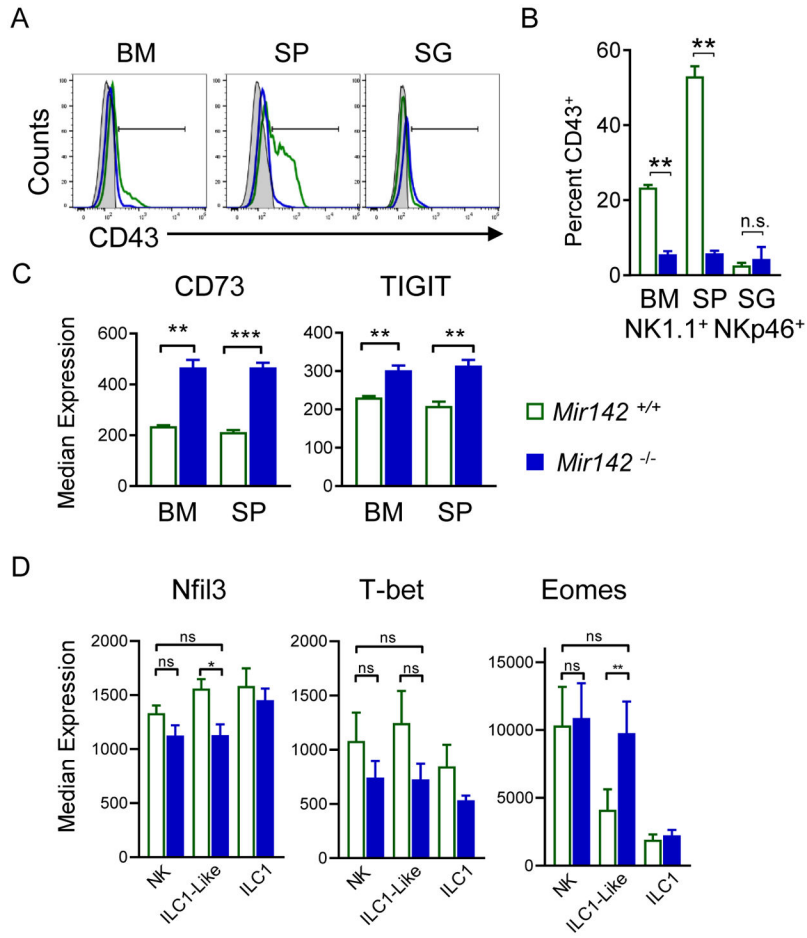
Figure 3. miR-142-deficient type-1 ILCs display ILC1-like phenotype in lymphoid tissues.
(**A**) Representative histograms depict CD43 expression on NK1.1$^+$NKp46$^+$ cells from
Mir142$^{-/-}$ (blue) mice compared to controls (green). Gray filled histograms represent
CD43$^-$ lymphocytes. (**B**) Summary from (A). (**C**) Summary CD73 and TIGIT median
expression on NK1.1$^+$NKp46$^+$ cells. (**D**) Transcription factor median expression on
Mir142$^{-/-}$ and control NK1.1$^+$NKp46$^+$ cells. Data are from 2-4 independent experiments
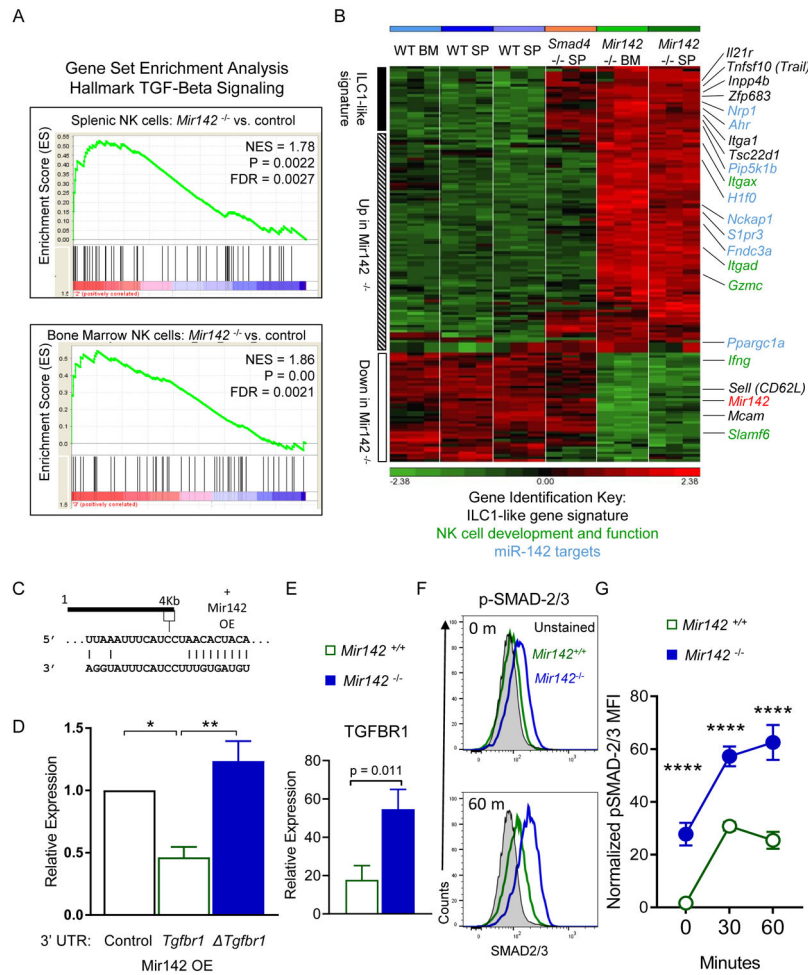with N=5-10 mice per group. Data were compared using Student's T or Mann Whitney tests.

Figure 4. TGF-β signaling is increased in *Mir142⁻/⁻* type-1 ILCs.
(**A-B**) CD3⁻NK1.1⁺NKp46⁺ cells were flow-sorted from *Mir142⁺/⁺* (WT) or *Mir142⁻/⁻*
(KO) BM or SP and microarray performed. (**A**) GSEA of the TGF-β Hallmark Signaling
Pathway gene set in *Mir142⁻/⁻* versus WT from SP and BM. NES, Normalized enrichment
score. (**B**) Heat map of differentially regulated genes between *Mir142⁺/⁺*, *Smad4 ⁻/⁻*, and
Mir142⁻/⁻ NK1.1⁺ cells. Genes associated with the ILC1-like signature (black), miR-142
targets (blue), and NK cell development and effector functions (green) are indicated. Data
are from 3 biological replicates. (**C**) Predicted miR-142-3p binding site in the 3'UTR of
Tgfbr1. (**D**) Luciferase reporter assay for miR-142 overexpression (OE) without the *Tgfbr1*
3'UTR (empty), with *Tgfbr1* 3' UTR (WT) or with *Tgfbr1*-mutated at the miR-142-3p
binding site in the 3' UTR (   ). Data summarize 3 independent experiments and were
compared using an ANOVA. (**E**) Summary TGFBR1 expression on type-1 ILCs from SP of
indicated mice (relative expression: median minus FMO); data from > 3 independent
experiments were compared with T test (n=6-8 mice per group). (**F-G**) SP cells were
stimulated with 10 ng/mL IL-15 plus 10 ng/mL TGF-β1 or left unstimulated (0 minutes) and
assessed for phosphorylated (p) SMAD-2 and/or −3. (**F**) Representative flow plot showing
pSMAD-2 and/or −3 in unstimulated (0m, top) or stimulated (60m, bottom) CD3⁻NK1.1⁺

cells. (**G**) Summary from (F). Data are from 2 independent experiments with 6-7 mice per group. Significance was determined by 2-Way ANOVA. Please also see Figure S4.
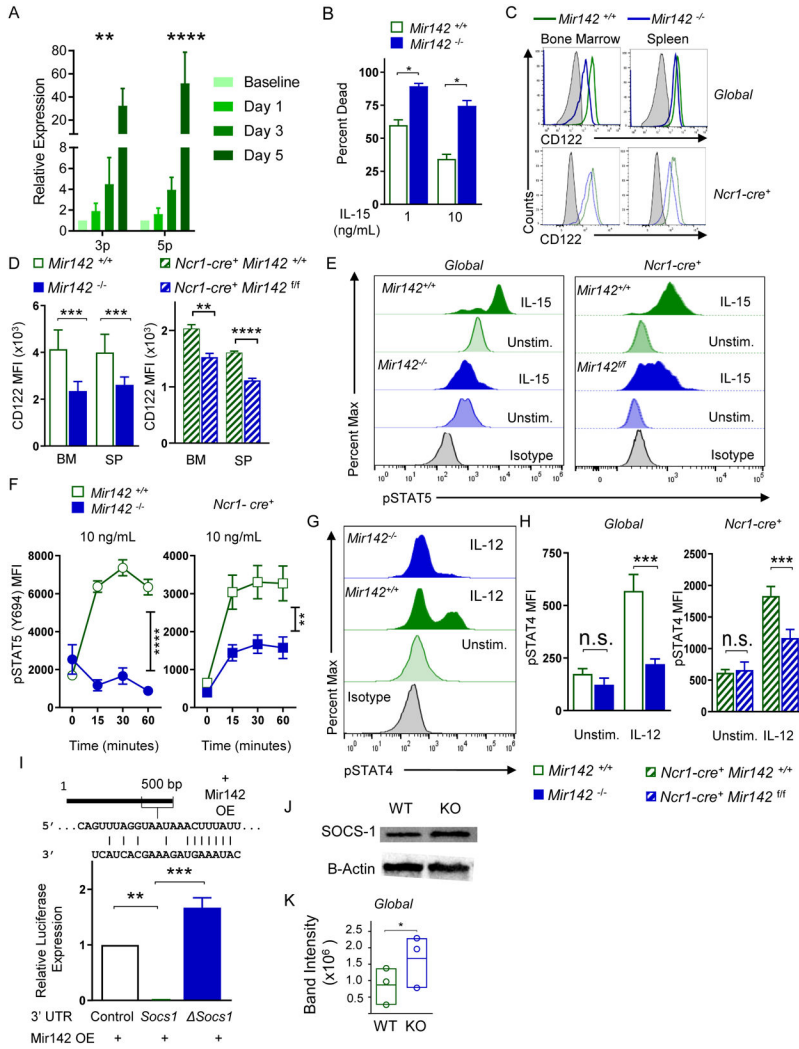
Figure 5. miR-142-deficient type-1 ILCs are hyporesponsive to IL-15 signaling.
(**A**) WT CD3−NK1.1+ cells were sorted from the SP and incubated with 10 ng/mL IL-15.
Immediately after sorting (baseline) and after stimulation, RNA was extracted from the cells
and miR-142-3p/5p expression were assessed by qPCR. Summary data (normalized to
baseline) from 2 independent experiments with 3 biological replicates. (**B**) Splenocytes were
incubated with IL-15 for 48 hours in vitro. Summary data depict the percent of type-1 ILCs
(CD45+CD3−NK1.1+) positive for 7-AAD and/or Annexin V. (**C**) Representative histograms
of surface expression of CD122 (IL-2 and −15Rβ) on *Mir142*+/+ and *Mir142*−/−
CD45+CD3−NK1.1+ cells *(Global,* Top) and *Ncr1-cre+ Mir142*+/+ and *Ncr1-cre+ Mir142*f/f
CD45+CD3−NK1.1+YFP+ cells (*Ncr1-cre+*, Bottom). Gray filled histograms depict CD122-
negative lymphocytes. (**D**) Summary data from (C) showing the MFI. (**E**) Representative
histograms showing intracellular pSTAT-5 (Y694) staining in *global* (left) and *Ncr1-cre+*
(right) NK1.1+ and/or YFP+ cells after 15-minute stimulation with IL-15. (**F**) Summary data
from (E). (**G**) Representative histograms showing pSTAT-4 in *global* (Top) and *Ncr1-cre+*
(Bottom) CD3− NK1.1+ and/or YFP+ cells after stimulation with IL-12 for 15 minutes. (**H**)
Summary data from (G). (**I**) Predicted miR-142-5p binding site in *Socs1* 3' UTR (top). A

luciferase reporter assay for *Socs1* 3'UTR. Data are compared using an ANOVA. Data summarize 3 independent experiments. (**J-K**) CD3$^-$NK1.1$^+$ SP cells from control and *Mir142$^{-/-}$* SP were sorted and assessed for Socs1 and β-actin by western blot. (**J**) Representative blot from 3 independent experiments showing Socs1 (top) and β-Actin (bottom). (**K**) Summary data depicting Socs1 band intensity (normalized using β-actin). Comparisons were made using RM-ANOVA (A, I), Student's T test/Mann-Whitney (B-D, H), RM-ANOVA (F), paired T test (K). Please also see Figure S5.
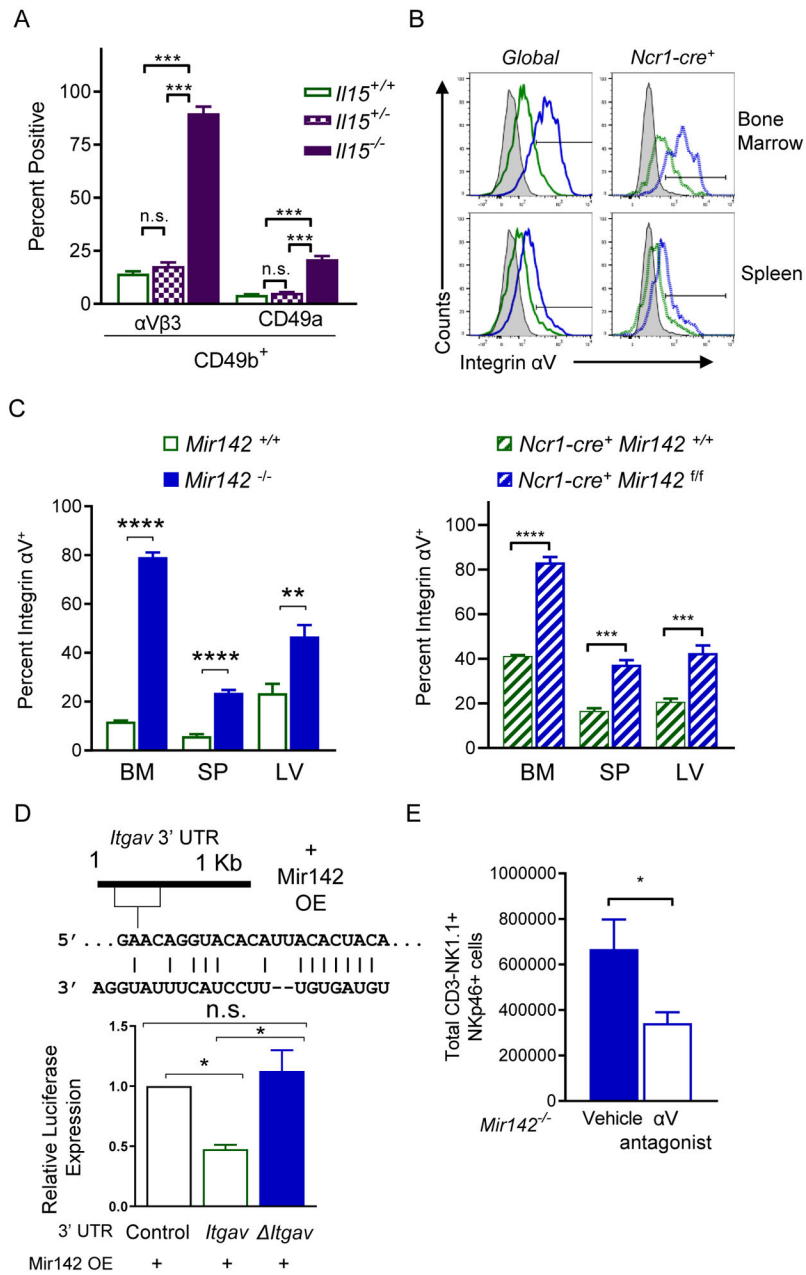
Figure 6. Integrin aV promotes type-1 ILC survival in miR-142-deficient mice.
(**A**) Summary data of integrin αVβ3 and CD49a on CD3⁻NK1.1⁺NKp46⁺CD49b⁺ cells
from the SP of *Il15⁻/⁻* or control mice. (**B**) Representative histogram showing integrin αV
expression in the indicated tissues of Global and *Ncr1-cre⁺* mice. (**C**) Summary showing
percent integrin αV⁺ NK1.1⁺NKp46⁺ cells in the indicated tissues from *Mir142⁻/⁻* (left),
Ncr1-cre⁺ Mir142^f/f (YFP⁺, right), and controls. (**D**) Predicted miR-142-3p binding site in
3'UTR of *Itgav* (top). Luciferase reporter assay for *Itgav* 3'UTR (bottom). Data summarize
3 independent experiments and were compared using an ANOVA. (**E**) *Mir142⁻/⁻* mice were
treated for 2 weeks with an αV inhibitor or vehicle. Summary data of total type-1 ILCs in

the SP from 4 independent experiments, n=11 mice per group. (C, E) Data were compared using Student's T test. See also Figure S3.
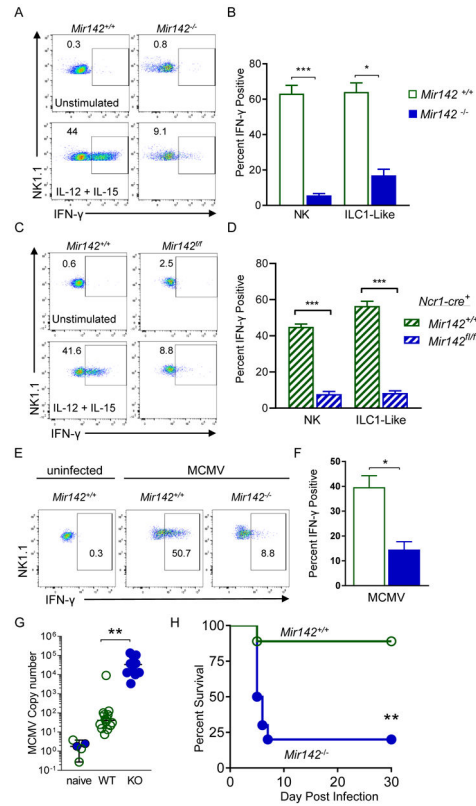
Figure 7. miR-142-deficient type-1 ILCs display altered effector responses in vitro and in vivo.
(**A-B**) Splenocytes from *Mir142*^{+/+} and *Mir142*^{−/−} mice were stimulated for 6 hours. (**A**) Representative flow plots showing intracellular IFN-γ staining in CD45^{+}CD3^{−}NK1.1^{+} cells. (**B**) Summary data from (A). (**C-D**) Splenocytes were isolated from *Ncr1-cre*^{+} *Mir142*^{+/+} (control, open green bars) and *Ncr1-cre*^{+} *Mir142*[f/f] (filled blue bars) mice and stimulated for 6 hours. (**C**) Representative flow plots showing intracellular IFN-γ staining in CD45^{+}CD3^{−}NK1.1^{+}YFP^{+} cells. (**D**) Summary data from (C). (**E-F**) 36 hours after MCMV infection, SP NK1.1^{+} cells were assessed immediately for intracellular IFN-γ protein by flow cytometry. (**E**) Representative flow plots showing IFN-γ in CD45^{+}CD3^{−}NK1.1^{+} cells. (**F**) Summary from (E). (**G**) Viral copy numbers in the SP of MCMV-naïve control, *Mir142*^{+/+} (WT) and *Mir142*^{−/−} (KO) MCMV-infected mice, were assessed using qPCR 4 days after infection (units: IE1×1000/B-Actin). (**H**) Mice were infected with 1e[5] PFU MCMV and survival assessed. Pooled data from 2-3 independent experiments with >4 mice per group per experiment. Comparisons were made using Student's T test or Mann-Whitney test, and log-rank (H). See also Figure S7.

KEY RESOURCES TABLE

REAGENT or RESOURCE	SOURCE	IDENTIFIER
Antibodies		
APC CD49b anti-mouse mAb (DX5)	Thermo Fisher	Cat #17-5971-82
eFluor660 CD107a anti-mouse mAb (1D4B)	Thermo Fisher	Cat #50-1071-82
PerCP-eFluor710 EOMES anti-mouse mAb (Dan11mag)	Thermo Fisher	Cat #46-4875-82
APC Granzyme B anti-human mAb (GB12)	Thermo Fisher	Cat #MHGB05
PE IFN gamma anti-mouse mAb (XMG1.2)	Thermo Fisher	Cat #12-7311-82
PE-Cyanine7 NKp46 anti-mouse mAb (29A1.4)	Thermo Fisher	Cat #25-3351-82
Alexa Fluor 647 Stat5 (pY694) mAb (47/Stat5(pY694))	BD Biosciences	Cat #562076
Brilliant Violet 605 anti-mouse CD45 mAb (30-F11)	BioLegend	Cat #103139
Brilliant Violet 605 anti-mouse CD45.1 mAb (A20)	BioLegend	Cat #110737
PE anti-rat/mouse CD49a mAb (Ha31/8)	BD Biosciences	Cat #562115
PerCP-Cy5.5 anti-mouse NK-1.1 mAb (PK136)	BD Biosciences	Cat #561111
PE rat anti-mouse CD43 mAb (S7)	BD Biosciences	Cat #553271
APC CY7 Hamster anti-mouse CD3e mAb (145-2C11)	BD Biosciences	Cat #557596
BV605 Hamster anti-rat/mouse CD49a mAb (Ha31/8)	BD Biosciences	Cat #740375
T-BET BV421 (4B10)	Biolegend	Cat #644815
PE Rat anti-mouse CD51 mAb (RMV-7)	BD Biosciences	Cat #551187
APC-CY7 mouse anti-mouse NK1.1 mAb (PK136)	BD Biosciences	Cat #560618
Pacific Blue Hamster anti-mouse CD3e mAb (500A2)	BD Biosciences	Cat #558214
NFIL3 (E4BP4), Alexa Flour® 647, Clone: 1218A	Fisher (R&D)	IC8888R100
Alexa Fluor 647mouse anti-STAT4 (pY693)	BD Biosciences	Cat #558137
Smad2(pS465/pS457)/Smad3(pS423/pS425) Mouse, PE, Clone: 072-670, BD	BD Biosciences	BDB562586
TGF-beta RI/ALK-5, APC, Clone: 141231, 100 tests	R&D Systems	FAB5871A100
Anti-Mouse CD73 eFluor 450 mAb (eBioTY/11.8)	eBioscience	Cat #48-0731-82
BV605 mouse anti-mouse TIGIT mAb (1G9)	BD Biosciences	Cat #744212
Anti-h/m AF488 IL12RB2	R&D systems	Cat #FAB1959G
PE Anti-mouse CD200R mAb (OXr2)	BioLegend	Cat #123907
Anti-mouse CD3e eFluor 450 mAb (145-2C11)	eBioscience	Cat #48-0031-82
NFIL3/E4BP4 Alexa Fluor 488	Fisher (R&D)	Cat# IC8888G
Pe/Cy7 anti-mouse CD127 (IL-7Ra) mAb (A7R34)	Biolegend	Cat #135014
Anti-mouse CD122 e Fluor 450 mAb (TM-b1)	eBioscience	Cat #48-1-222-82
FITC Hamster anti-mouse CD3e mAb (145-2C11)	BD Biosciences	Cat #553062
FITC mouse anti-mouse NK1.1 mAb (PK136)	BD Biosciences	Cat #553164
Anti-Hu/MO CD45R (B220) FITC mAb (RA3-6B2)	Thermo Fisher	Cat #11-0452-82
PE Hamster anti-mouse CD11c mAb (HL3)	BD Bioscience	Cat #553802
APC anti-mouse CD283 TLR3 mAb (11F8)	Biolegend	Cat #141906
APC CY7 Anti-mouse CD8a mAb (53-6.7)	Biolegend	Cat #100714

REAGENT or RESOURCE	SOURCE	IDENTIFIER
Anti-m TGFBR1/ALK5 APC	R&D systems	Cat #FAB5871A
PE/CY7 anti-mouse/rat CD61 mAb (HMb3-1)	Biolegend	Cat #104317
APC Ly-49H anti-mouse mAb (3D10)	Thermo Fisher	Cat# 17-5886-82
PE Anti Mouse CD218a IL-18Ra mAb (P3TUNYA)	eBioscience	Cat# 12-5183-82
APC CY7 Rat anti-mouse CD11b mAb (M1/70)	BD Biosciences	Cat# 557657
SOCS1 (A156) Antibody	Cell Signaling	Cat# 3950S
STREPTAVIDIN PE	BD Bioscience	Cat# 554061
PE mouse anti-mouse CD212	BD Biosciences	Cat# 551974
PE Rat anti-mouse CD132	BD Biosciences	Cat# 554457
anti-CD29, FITC, Clone: Ha2/5, BD	BD Biosciences	BDB561796
FITC Rat anti-mouse CD43 mAb (s7)	BD Biosciences	Cat# 553270
FITC anti-mouse LY49D mAb (49-h4)	Biolegend	Cat#138605
APC anti-mouse NKG2D mAb (CX5)	eBioscience	Cat# 17-5882-82
PE Anti-mouse NKG2A b6 mAb (16a11)	Ebioscience	Cat# 12-5897-82
E450 anti-mouse/rat KI67 mAb (SolA15)	eBioscience	Cat# 48-5698-82
FITC Rat anti-mouse Ly-6G and Ly-6C GR1 mAb (RB6-8C5)	BD Bioscience	Cat# 553127
FITC Rat anti-mouse TER119/Erythroid Cells mAb (TER-119)	BD Biosciences	Cat# 557915
APC Rat anti-mouse CD135 FLT3 mAb (A2F10.0)	BD Biosciences	Cat# 560718
PE anti-mouse CD94 mAb (18d3)	eBioscience	Cat# 12-0941-81
Bacterial and Virus Strains		
MCMV Smith Strain	French Lab	
Chemicals, Peptides, and Recombinant Proteins		
Mouse IL-3	Peprotech	Cat# 213-13
mouse IL-15	Peprotech	Cat# 210-15
Mouse IL-12	Peprotech	Cat# 210-12
Recombinant Human TGF-B1 (HEK293 derived), 10ug	Peprotech	Cat# 100-21
RPMI1640	GE Healthcare Life Science	Cat# SH30027.02
Fetal Bovine Serum (FBS)	Sigma	Cat # F2442
Pen Strep	GE Healthcare Life Science	Cat# SV30010
NEAA	GE Healthcare Life Science	Cat# SH30027.02
Sodium Pyruvate	GE Healthcare Life Science	Cat# SH30239.01
L-Glutamine	Hyclone	Cat# SH30239.01
HEPES	GE Healthcare Life Science	Cat# SH30237.01
fixation/permeabilization kit	BD Bioscience	Cat# 51-2090KZ
fixation/permeabilization concentrate	Invitrogen	Cat# 00-5123-43
fixation/permeabilization diluent	Invitrogen	Cat# 00-5223-56
Trizol	Ambion Life Technologies	Cat# 15596026
poly I:C	Invitrogen	Cat # tlrl-pic
7AAD	Sigma	Cat# A9400

REAGENT or RESOURCE	SOURCE	IDENTIFIER
Cell Trace Violet	Thermo Fisher	C34557
Cell Trace Yellow	Thermo Fisher	C34567
Phosphate Buffer Saline (PBS)	Hyclone	Cat# SH30028.03
Collagenase	Sigma	Cat# C9407-100MG
DNase	Sigma	Cat # D4527-10KU
Percoll	GE Healthcare	17-0891-01
1X HBSS	Gibco	14025-076
CFSE	Sigma	21888-25MG-F
10x PBS	Fisher Scientific	BP3991
Ammonium chloride, 500G	Sigma	A9434-500G
Potassium Chloride, 500g, for molecular biology	Sigma	P9541-500G
Electron Microscopy Sci. 16% Paraformaldehyde Aq Sol., Case of 10	Fisher	50-980-489
DMEM Media	Gibco	11965
DMSO	Sigma	D2650
EDTA	Corning	46-034-CL
Heparin	Fresenius Kabi USA	401807K
AO/PI	Nexcelom	CS2-0106-5ML
Ethyl Alcohol 200 Proof	Pharmco	Cat #11100020S
Critical Commercial Assays		
EasySep™ Mouse NK Cell Isolation Kit	Stem Cell Technologies	Catalog # 19855
Direct-zol RNA Microprep	Zymo Research	R2061
PE Annexin V Apoptosis Detection Kit	BD Bioscience	Catalog No. 559763
Automacs NK Cell Isolation Kit	Miltenyi	
CellTrace™ Yellow Cell Proliferation Kit, for flow cytometry	Thermo Fisher	
CellTrace™ Violet Cell Proliferation Kit, for flow cytometry	Thermo Fisher	C34557
Promega Dual-Glo Luciferase Assay System, 10mL	Thermo Fisher	PR-E2920
Deposited Data		
MicroArray	GEO	GSE85476
Experimental Models: Cell Lines		
Mouse: 3T3	ATCC	
Human: 293T	Sands Lab	
Experimental Models: Organisms/Strains		
Mouse: $Mir142^{-/-}$	Reddy Lab	n/a
Mouse: $Mir142^{f/f}$	Bolden Lab	n/a
Mouse: CD45.2 C57BL/6J	The Jackson Laboratory	Cat# JAX: 000664
Mouse: CD45.1 C57BL/6J	The Jackson Laboratory	Cat# JAX: 002014
Mouse: Ncr1-icre	Vivier Lab	
Mouse: $Il15^{-/-}$	Li Lab	
Oligonucleotides		

REAGENT or RESOURCE	SOURCE	IDENTIFIER
has-miR-142-3p, S(50RT/150 PCR rxns)	Life Technologies	000464
has-miR-142-5p, S(50RT/150 PCR rxns)	Life Technologies	002248
snoRNA135, TaqMan microRNA control Assay, S(50RT/150 PCR rxns)	Life Technologies	001230
Software and Algorithms		
FlowJo	Treestar Inc	
Automacs	Miltenyi Biotec	
Cellometer	Nexcelom	
GraphPad Prism 8	GraphPad	
Image Lab	BioRad	